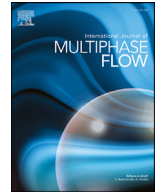




ELSEVIER

Contents lists available at ScienceDirect

## International Journal of Multiphase Flow

journal homepage: [www.elsevier.com/locate/ijmulflow](http://www.elsevier.com/locate/ijmulflow)Development of a drift-flux velocity closure for a coupled  $\Sigma$ -Y spray atomization modelA. Pandal<sup>a,\*</sup>, B.M. Ninge Gowda<sup>b</sup>, F.N.Z. Rahantamialisoa<sup>b</sup>, J. Zembí<sup>b</sup>, H.G. Im<sup>c</sup>, M. Battistoni<sup>b</sup><sup>a</sup> Departamento de Energía (Área de Mecánica de Fluidos), Universidad de Oviedo, Spain<sup>b</sup> Università degli Studi di Perugia, Department of Engineering, Italy<sup>c</sup> King Abdullah University of Science and Technology, Saudi Arabia

## ARTICLE INFO

## Article history:

Received 14 August 2020

Revised 23 February 2021

Accepted 13 May 2021

Available online 17 May 2021

## Keywords:

Eulerian Spray atomization

Interface surface density

Drift-Flux

Diesel spray

CFD

OpenFOAM®

## ABSTRACT

Modeling of spray in a dense near-nozzle region remains a great challenge, because of the large scale separation between the small features of the interface and the overall jet. Diffuse-interface treatment in a single-fluid Eulerian framework, in which the interfacial surface area density ( $\Sigma$ ) is used to describe the atomization process, has attracted interest for its potential in providing a manageable and still accurate model. In this work, we propose a new formulation of the  $\Sigma$ -Y spray atomization model that accounts for liquid diffusion due to drift-flux velocities, correctly predicting the behavior under all relevant engine conditions. Additionally, the present formulation allows the interfacial dynamics to impact the transport of the liquid mass fraction, thus making the interfacial density an active scalar fully coupled with the rest of the flow, overcoming limitations of previous formulations. The new model is implemented in the OpenFOAM framework and validated against experimental measurements under non-vaporizing and vaporizing environments, and at reacting conditions.

© 2021 Elsevier Ltd. All rights reserved.

## 1. Introduction

Improving engine and real combustion systems performance requires advanced spray and combustion models in order to reduce pollutants formation and comply with the increasingly tight emission regulations. This goal is extremely challenging for scientists due to the interaction of complex physical and chemical phenomena, such as the injection of high-pressure liquid fuel, atomization, evaporation, fuel-air mixture and combustion, that are still not well understood (Gorokhovski and Herrmann, 2008; Schmidt and Corradini, 2001), while they are fundamental factors in the overall performance of propulsion systems.

In particular, the difficulty lies in the fact that the atomization process of the liquid phase occurs at extremely small length scales and high speeds in current injection systems, which is a great limitation to the experimental characterization of the spray, especially in the near-nozzle region. The problem is easily noticed by observing that typically available diesel spray measurements concern tip penetration and spray cone angle (macroscopic characteristics of diesel sprays) (Desantes et al., 2006; Mo et al., 2016) and droplet size measurements conducted at a minimum axial distance from

the injector orifice in the range of 12 mm (Guan et al., 2015; Jedelsky et al., 2018; Payri et al., 2008). The optically dense spray zone is hardly penetrable with standard diagnostic techniques, and thus few experimental results are available. The dense region within the first few millimeters of the injector is only penetrable with special diagnostics such as x-ray radiography (Kastengren et al., 2017; Pickett et al., 2014) (offering mass distribution and average SMD only), preventing a clear flow characterization and the development of predictive primary atomization models.

Modeling spray atomization can be accomplished employing many different approaches. In general, it is desirable to simulate the spray behavior from first principles, formulated solely on basic conservation laws instead of introducing engineering modeling assumptions. Advanced spray models based on Eulerian approaches, such as the volume-of-fluids (VoF) and level-set (LS) techniques, have clearly emerged in the recent years. However, such approaches (Lebas et al., 2009; Shin et al., 2017) while provide the highest details of the liquid-gas interface information, still demand extreme levels of computational resources, preventing their use at device-scale simulations. On the opposite side, one can trust the commonly used Lagrangian discrete droplet method (DDM) (Dukowicz, 1980), in which the liquid phase is described as Lagrangian parcels moving and interacting with the surrounding gas phase described in an Eulerian reference frame. Lagrangian particle tracking is the classic approach for engine simulations due

\* Corresponding author.

E-mail address: [pandaladrian@uniovi.es](mailto:pandaladrian@uniovi.es) (A. Pandal).

to its computational efficiency, but it is inadequate for dense two-phase flows in the near nozzle region of compression ignition engines (Battistoni et al., 2018), since the dense spray core cannot be properly represented and the method shows great mesh dependency and suffers from limitations of the CFD cell resolution (Lee and Reitz, 2013).

This dilemma is discussed in recent studies (Battistoni et al., 2019; Desantes et al., 2020b; Ma et al., 2019; Pandal et al., 2018; 2016), which use a diffuse-interface method within a fully Eulerian framework with great performance in simulating fuel spray physics. In such a problem, considering that not all scales can be solved, by applying a filter either explicitly (RANS, LES approaches) or implicitly through a mesh resolution that cannot ensure that all scales are solved, a smooth continuous transition between phases is recovered (thus including intermediate states). The end result is a diffuse-interface treatment in an Eulerian framework, where unresolved interface features are modeled instead of being tracked. Therefore, flow scale separation is assumed between the large scale features and the atomization process occurring at the smaller scales, as initially proposed by Vallet and Borghi (1999), Vallet et al. (2001). As a consequence, liquid dispersion is assumed to be governed by the turbulent mixing of a variable density fluid, while atomization is modeled by the surface density concept, which represents the phase interfacial area per unit of volume. As a result, these models are based on two scalar transport equations: one for the liquid (or gas) phase mass fraction,  $Y$ , and the other for the interfacial surface density,  $\Sigma$ , hence referred to as the  $\Sigma$ - $Y$  model (fully Eulerian), in contrast to ELSA (Eulerian-Lagrangian Spray Atomization), which includes a transition to Lagrangian particle tracking (Blokkeel et al., 2003).

After the atomization occurs within the dense region of the spray, this model can also describe the evaporation process of the liquid fuel surrounded by high-temperature and pressure ambient gases. This is an additional advantage of the  $\Sigma$ - $Y$  model. The experimental findings by Siebers (1998, 1999, 2008) reported that turbulent mixing and gas entrainment may be the dominant mechanism for diesel spray vaporization, hence referred to as the 'mixing-controlled evaporation.' In addition, more recent investigations (Crua et al., 2017; Dahms et al., 2013; Dahms and Oefelein, 2015) showed that in-cylinder conditions for diesel fuel injection can even promote a transition to diffusive mixing, in very hot conditions and for very high pressure levels (Crua et al., 2017), where diffuse interfaces between gas and liquid appear, instead of well-defined liquid-vapor interfaces within the drop cloud. So, the diffuse-interface approach which is considered in this work for two-phase flow regimes, in principle has also the potential to be extended to trans- and supercritical applications, provided that specific sub-models for mass, momentum and heat transfer are developed.

Although the current  $\Sigma$ - $Y$  model have shown good performance for diesel sprays under normal engine operating conditions, i.e., at high injection pressure and chamber gas density, the underlying feature of strong coupling between phases becomes invalid at lower ambient density and injection pressure (García-Oliver et al., 2013). In addition, the model formulation, based on the passive scalar  $\Sigma$ , has raised some criticisms in the literature for relying solely on the turbulent mixing independently of the atomization evolution. These concerns compromised their extensive use and motivates further modeling improvements. In fact, there have been some attempts (Andreini et al., 2016; Beau et al., 2005; 2004) to extend the model to recover each phase velocity from the mixture velocity to properly represent the turbulent liquid flux. However, a strong basis for such developments was not provided.

In the present contribution, a new formulation for fully Eulerian  $\Sigma$ - $Y$  atomization model that accounts for diffusion due to drift-flux velocities is presented, which is especially relevant in high den-

sity ratio flows. The model is implemented in the OpenFOAM CFD open source C++ library (Weller et al., 1998). The fidelity of the new model is evaluated at diesel engine conditions by validation against experimental measurements under non-vaporizing and vaporizing environments, and including applications to reacting conditions.

The results show improved predictive capability under a wider range of engine conditions, allowing the interfacial dynamics to affect the transport of the liquid fraction, fully coupled with the gas flow.

## 2. Spray model description

### 2.1. Coupled $\Sigma$ - $Y$ model description

The classic  $\Sigma$ - $Y$  model considers the liquid-gas mixture as a pseudo-fluid with a single velocity field. Additionally, considering that the flow exiting the injector is operating at large Reynolds and Weber numbers, it is possible to assume a separation of the large scale flow features, such as mass transport, from the atomization process occurring at smaller scales. This allows the direct simulation of the large scale bulk transport of the liquid while unresolved liquid turbulent transport is traditionally modeled using simple closures such as the linear constitutive law based on the concentration gradient for turbulent diffusion.

In contrast, in the present formulation, the single-fluid model with a single velocity is still used but taking into account the additional macroscopic effect on the liquid dispersion due to the drift velocities. The  $\Sigma$ - $Y$  model originates from the work of Vallet and Borghi (1999), and it is formulated following an analogy with gas-phase turbulent species mixing and combustion, but applied to two-phase flows, therefore neglecting slip effects.

To introduce the present model formulation and to provide a broader perspective, in this work the rigorous conservation equations, based on the theory of two-phase flow mixtures, are used (Ishii and Hibiki, 2006), as the starting point for the atomization model derivation. This two-phase single-fluid model discussed hereafter is also referred to as drift-flux model (Ishii and Hibiki, 2006), and it is appropriate for mixtures where the dynamics of two phases are coupled, therefore deemed suitable for diesel spray applications.

Following the fundamental work of Ishii and Hibiki (2006), the averaged balance equations for a turbulent, compressible, two-phase mixture, are written as

*Mixture continuity equation*

$$\frac{\partial \rho_m}{\partial t} + \nabla \cdot (\rho_m \mathbf{v}_m) = 0 \quad (1)$$

*Secondary (dispersed) phase continuity equation*

$$\frac{\partial \bar{\rho}_2 \alpha_2}{\partial t} + \nabla \cdot (\bar{\rho}_2 \alpha_2 \mathbf{v}_m) = -\nabla \cdot (\bar{\rho}_2 \alpha_2 \mathbf{v}_{2m}) - \Gamma_{evap} \quad (2)$$

*Mixture momentum equation*

$$\frac{\partial \rho_m \mathbf{v}_m}{\partial t} + \nabla \cdot (\rho_m \mathbf{v}_m \mathbf{v}_m) = -\nabla p_m + \nabla \cdot (\boldsymbol{\tau} + \boldsymbol{\tau}^T + \boldsymbol{\tau}^D) + \rho_m \mathbf{g}_m + \mathbf{M}_m \quad (3)$$

*Mixture energy equation, in terms of enthalpy*

$$\frac{\partial \rho_m h_m}{\partial t} + \nabla \cdot (\rho_m h_m \mathbf{v}_m) = \nabla \cdot (\mathbf{q} + \mathbf{q}^T + \mathbf{q}^D) + \sum_{k=1}^2 \alpha_k \mathbf{v}_{km} \cdot \nabla \bar{p}_k + \frac{Dp_m}{Dt} + \phi_m^\mu + \phi_m^\sigma + \phi_m^i \quad (4)$$

The first two equations represent the conservation of total mass and of the secondary phase mass, where  $\rho_m$  is the mixture density,  $\mathbf{v}_m$  is the mixture center of mass velocity,  $\alpha_2$  is the liquid

(secondary phase) volume fraction,  $\bar{\rho}_2$  is the liquid phase averaged density,  $\Gamma_{evap}$  is the phase change source term and  $\mathbf{V}_{2m}$  is the diffusion velocity of the liquid with respect to the mass center of the mixture.

The third equation is the mixture momentum equation, where  $p_m$  is the mixture pressure,  $\boldsymbol{\tau}$  is the average viscous stress,  $\boldsymbol{\tau}^T$  is the turbulent stress,  $\boldsymbol{\tau}^D$  is the diffusion stress,  $\mathbf{g}_m$  expresses body accelerations on the mixture and  $\mathbf{M}_m$  is the mixture momentum source due to the surface tension effects.

Similarly, the fourth equation is the energy balance for the mixture, expressed in terms of mixture enthalpy  $h_m$ . In this equation  $\mathbf{q}$  is the average conduction heat flux,  $\mathbf{q}^T$  is the turbulent heat flux,  $\mathbf{q}^D$  is the heat flux due to phase diffusion, and  $\bar{p}_k$  is the  $k$ th phase average pressure. The remaining terms collectively express the work done by viscous dissipations,  $\phi_m^\mu$ , the work done by surface tension forces,  $\phi_m^o$ , and the interfacial mechanical energy transfer,  $\phi_m^i$ .

It is worth remarking that the above equations are already time (or ensemble) averaged, therefore they already include turbulent fluxes, resulting from averaging the products of fluctuating quantities. Specifically, these terms are  $\mathbf{V}_{2m}$ ,  $\boldsymbol{\tau}^T$ ,  $\mathbf{q}^T$ , in the dispersed phase continuity, momentum, and energy equations, respectively (Ishii and Hibiki, 2006).

This set of equations constitute the full drift-flux model. Quite often, however, some terms, whose closure could also be extremely complex, are fortunately negligible (Ishii and Hibiki, 2006). In particular, neglecting the effect of surface tension on the mixture dynamics, the pressure jump across the interface can be neglected and phase pressure  $\bar{p}_k$  and mixture pressure  $p_m$  become the same, therefore now on denoted simply as  $p$ . In addition, in the preset work, it is assumed that the surface tension effects  $\phi_m^o$  and the mechanical energy effects  $\phi_m^i$  on the energy balance are small, therefore neglected. These arguments also allow to neglect the momentum source  $\mathbf{M}_m$  because of its small contribution to the momentum balance.

Diffusion fluxes deserve some more details. These are formulated as follows:

$$\boldsymbol{\tau}^D = - \sum_{k=1}^2 \alpha_k \bar{\rho}_k \mathbf{V}_{km} \mathbf{V}_{km} = - \frac{\alpha_2}{1 - \alpha_2} \frac{\bar{\rho}_1 \bar{\rho}_2}{\rho_m} \mathbf{V}_{2j} \mathbf{V}_{2j} \quad (5)$$

$$\mathbf{q}^D = - \sum_{k=1}^2 \alpha_k \bar{\rho}_k \hat{h}_k \mathbf{V}_{km} = - \alpha_2 \frac{\bar{\rho}_1 \bar{\rho}_2}{\rho_m} (\hat{h}_2 - \hat{h}_1) \mathbf{V}_{2j} \quad (6)$$

where  $\hat{h}_k$  is  $k$ th phase mass weighted enthalpy. The first formulation represents the fluxes definition, while the second expression on the right is obtained by using kinematics relations and having introduced the concept of drift velocity  $\mathbf{V}_{2j} = \hat{\mathbf{v}}_2 - \mathbf{j}$  as the difference between the dispersed phase mass weighted velocity  $\hat{\mathbf{v}}_2$  and the mixture volumetric flux  $\mathbf{j}$  (namely, the velocity of the center of volume).

The drift velocity term needs a specific closure model, which is based on the work of Manninen et al. (1996). In particular, this drift velocity is related to the relative velocity,  $\mathbf{v}_{21}$ , as:

$$\mathbf{V}_{2j} = (1 - \alpha_2) \cdot (\hat{\mathbf{v}}_2 - \hat{\mathbf{v}}_1) = (1 - \alpha_2) \cdot (\mathbf{v}_{21}) \quad (7)$$

The kinematic constitutive equation used to obtain the relative velocity can be derived by combining the momentum equations of the dispersed phase and of the mixture (Manninen et al., 1996). Considering that the phase pressures are equal and that the additional force acting on the dispersed phase, created by density differences, is balanced by the drag force, the equation for the relative velocity can be derived (Manninen et al., 1996). However, the obtained expression presents some turbulent terms and due to that, a practical constitutive law is required. Then, the linear solution proposed by Ishii and Hibiki (2006) and Simonin (1990), for diluted

dispersed flows, is used:

$$\mathbf{v}_{21} = \mathbf{v}_{21,0} - D_{2m} \frac{\nabla \alpha_2}{\alpha_2} \quad (8)$$

As it can be seen, the relative velocity comprises two contributions, one expressing the terminal velocity of the particle phase in an infinite medium,  $\mathbf{v}_{21,0}$ , (whose closure will be discussed later, in Section 2.2) and a diffusion flux formulated through the gradient of the dispersed phase volume fraction and a diffusion coefficient of the secondary phase with respect to the mixture,  $D_{2m}$ . The diffusion coefficient is taken as the turbulent kinematic viscosity ( $\nu_t$ ) over a Schmidt number ( $S_c$ ).

By introducing the simplifications previously mentioned, and expressing the macroscopic phase diffusion terms through the drift velocities, and using  $\mathbf{V}_{2m} = (\bar{\rho}_1/\rho_m)\mathbf{V}_{2j}$ , the final form of the drift-flux model can be obtained. Additionally, the drift velocity closure, through the relative velocity, is substituted into the balance equations and the final form reads as follows

Mixture continuity equation

$$\frac{\partial \rho_m}{\partial t} + \nabla \cdot (\rho_m \mathbf{v}_m) = 0 \quad (9)$$

Secondary (dispersed) phase continuity equation

$$\begin{aligned} \frac{\partial \bar{\rho}_2 \alpha_2}{\partial t} + \nabla \cdot (\bar{\rho}_2 \alpha_2 \mathbf{v}_m) = & - \nabla \cdot \left[ \underbrace{\alpha_2 \frac{\bar{\rho}_1 \bar{\rho}_2}{\rho_m} (1 - \alpha_2) \mathbf{v}_{21,0}}_{\text{Extra Term due to Drift I}} \right] \\ & + \nabla \cdot \left[ \underbrace{\alpha_2 \frac{\bar{\rho}_1 \bar{\rho}_2}{\rho_m} (1 - \alpha_2) D_{2m} \nabla \alpha_2}_{\text{Extra Term due to Drift II}} \right] - \Gamma_{evap} \end{aligned} \quad (10)$$

It should be noted that  $\alpha_2 \bar{\rho}_2 = \rho_m \tilde{Y}_2$ , where  $\tilde{Y}_2$  is the liquid mass fraction. In view of this, the secondary phase transport equation can also be seen equivalently as the transport equation for the liquid mass fraction.

Mixture momentum equation

$$\begin{aligned} \frac{\partial \rho_m \mathbf{v}_m}{\partial t} + \nabla \cdot (\rho_m \mathbf{v}_m \mathbf{v}_m) = & - \nabla p + \nabla \cdot (\boldsymbol{\tau} + \boldsymbol{\tau}^T) \\ & - \nabla \cdot \left( \underbrace{\alpha_2 \frac{\bar{\rho}_1 \bar{\rho}_2}{\rho_m} (1 - \alpha_2) \mathbf{v}_{21,0} \mathbf{v}_{21,0}}_{\text{Extra Term due to Drift}} \right) \\ & + \rho_m \mathbf{g}_m \end{aligned} \quad (11)$$

Mixture energy equation, in terms of enthalpy

$$\begin{aligned} \frac{\partial \rho_m h_m}{\partial t} + \nabla \cdot (\rho_m h_m \mathbf{v}_m) = & \nabla \cdot (\mathbf{q} + \mathbf{q}^T) \\ & - \nabla \cdot \left( \underbrace{\alpha_2 \frac{\bar{\rho}_1 \bar{\rho}_2}{\rho_m} (\hat{h}_2 - \hat{h}_1) (1 - \alpha_2) \mathbf{v}_{21,0}}_{\text{Extra Term due to Drift I}} \right) \\ & + \alpha_2 \frac{\bar{\rho}_1 - \bar{\rho}_2}{\rho_m} (1 - \alpha_2) \mathbf{v}_{21,0} \cdot \nabla p \\ & \underbrace{\hspace{10em}}_{\text{Extra Term due to Drift II}} \\ & + \frac{Dp}{Dt} + \phi_m^\mu \end{aligned} \quad (12)$$

Where  $\rho_m = \alpha_1 \bar{\rho}_1 + \alpha_2 \bar{\rho}_2$ ,  $\mathbf{v}_m = (\alpha_1 \bar{\rho}_1 \hat{\mathbf{v}}_1 + \alpha_2 \bar{\rho}_2 \hat{\mathbf{v}}_2)/\rho_m$ , and  $h_m = (\alpha_1 \bar{\rho}_1 \hat{h}_1 + \alpha_2 \bar{\rho}_2 \hat{h}_2)/\rho_m$ .

According to Manninen et al. (1996), in the momentum and energy balance a further approximation is made by writing the diffusion stress in terms of  $\mathbf{v}_{21,0}$  only, and neglecting the second order contribution of the diffusion component. On the contrary, since

predicting liquid dispersion is of utmost importance in the current investigation, both terminal velocity and diffusion gradient terms are retained in the continuity equation of the dispersed phase (see Eq (10)). Here, it is very important to note that the diffusion term formulated through the gradient of  $\alpha_2$  (Extra Term due to Drift II) is analogous to the classical closure used for modeling gas phase molecular and turbulent mixing, and as generally found in the classic  $\Sigma$ -Y formulation. However, compared to that approach, using the rigorous two-phase flow theory an additional dispersion term arises, which will constitute the leading theme of this work.

Regarding the treatment of the phases (liquid and gas), an equation of state is then assigned to each phase to calculate the corresponding density. The gas phase obeys an ideal gas law, while for the liquid phase, density is calculated following the Hankinson-Brobst-Thomson (HBT) correlation (Reid et al., 1987), in which the liquid density is a function of temperature ( $T$ ) and pressure ( $p$ ).

In order to account for spray evaporation, an additional transport equation for vapor fuel mass fraction and also a procedure for calculating the source term,  $\Gamma_{evap}$ , of Eq. (10) have to be added (García-Oliver et al., 2013). The transport equation can be written in a similar way to the conservation of liquid fuel as:

$$\frac{\partial \rho_m \tilde{Y}_v}{\partial t} + \nabla \cdot (\rho_m \mathbf{v}_m \tilde{Y}_v) = \nabla \cdot (\rho_m D_Y \nabla \tilde{Y}_v) + \Gamma_{evap} \quad (13)$$

Again the same standard turbulent gradient law is used for closure in this transport equation. The sink/source terms for fuel liquid/vapor transport equations are calculated in terms of a rate needed to achieve the local adiabatic saturation conditions. This can be written as

$$\Gamma_{evap} = \rho_m \frac{Y_{v,sat} - \tilde{Y}_v}{\tau_{evap}} \quad (14)$$

where  $\tilde{Y}_v$  is the local vapor fuel mass fraction,  $Y_{v,sat}$  is the value of vapor fuel mass fraction under adiabatic saturation conditions and  $\tau_{evap}$  is a relaxation time set equal to the computational time step (Desantes et al., 2020b; Pandal et al., 2020a). Finally,  $Y_{v,sat}$  is calculated by means of a Locally Homogeneous Flow (LHF) approach (Faeth, 1983), considering the mixing-controlled assumption (Siebers, 1999). According to that, state relationships are applied to describe spray thermodynamic conditions under the assumption of local thermodynamic equilibrium.

To close the above system of equations, the temperature is obtained from a bulk mixture enthalpy equation, under the assumption of local thermodynamic equilibrium:

$$\begin{aligned} h_m(T) &= Z \cdot \hat{h}_2(T_0) + (1 - Z) \cdot \hat{h}_1(T_a) \\ &= \tilde{Y}_2 \cdot \hat{h}_{f,l}(T) + \tilde{Y}_v \cdot \hat{h}_{f,v}(T) \\ &\quad + (1 - \tilde{Y}_2 - \tilde{Y}_v) \cdot \hat{h}_a(T) \end{aligned} \quad (15)$$

where  $Z = \tilde{Y}_2 + \tilde{Y}_v$  is the mixture fraction.  $\hat{h}_{f,l}$ ,  $\hat{h}_{f,v}$  and  $\hat{h}_a$  denote the enthalpy of the liquid and vapor fuel and the ambient gas phase, respectively. For the vapor fuel and the ambient gas, enthalpies are derived from the respective specific heat capacities at constant pressure evaluated from 7-coefficients NASA polynomials. After that, for the liquid fuel the enthalpy of vaporization  $\Delta H_v$  is considered, as obtained from the corresponding states correlation by Pitzer et al. (1955). Being  $h_m$  the static enthalpy already obtained by solving Eq. (12).

The solution of the above transport equations fully characterizes the macroscopic mixture field, while the small-scale atomization is modeled by solving a transport equation for the evolution of the density of the interfacial surface area ( $\Sigma$ ). This last quantity is defined as the liquid surface present per unit volume at a given time and spatial position. Following the equation adopted by Vallet and Borghi (1999), on which nearly all the models in the literature are based, and applying a procedure analogous to the one used for the

mass transport equation, the subsequent transport equation for  $\Sigma$  within the drift-flux model is derived Eq. (16):

$$\begin{aligned} \frac{\partial \tilde{\Sigma}}{\partial t} + \nabla \cdot (\mathbf{v}_m \tilde{\Sigma}) &= \nabla \cdot (D_\Sigma \nabla \tilde{\Sigma}) + C_\Sigma \tilde{\Sigma} \left( 1 - \frac{\tilde{\Sigma}}{\tilde{\Sigma}_{eq}} \right) \\ &\quad + S_{\Sigma_{evap}} + S_{\Sigma_{init}} - \underbrace{\nabla \cdot \left( \tilde{\Sigma} \frac{\bar{\rho}_1}{\rho_m} \mathbf{v}_{2j} \right)}_{\text{Extra Term due to Drift}} \end{aligned} \quad (16)$$

In this equation the unclosed terms (generation and destruction) are treated through the restoration to an equilibrium value ( $\tilde{\Sigma}_{eq}$ ). Once again, a gradient law closure is used for the turbulent diffusion flux term, where  $D_\Sigma$  is the diffusion coefficient taken as the turbulent kinematic viscosity ( $\nu_t$ ) over a Schmidt number ( $Sc_\Sigma$ ). The  $S_{\Sigma_{evap}}$  term appears because of the change in the interphase surface as a result of fuel evaporation and is modelled as in Lebas et al. (2009). Then, the coefficient  $C_\Sigma$  is modeled as the inverse of the turbulent time scale:

$$C_\Sigma = C_1 \frac{\tilde{\epsilon}}{k} \quad (17)$$

While  $\tilde{\Sigma}_{eq}$  is set by the model proposed by Duret et al. (2013):

$$\tilde{\Sigma}_{eq} = C_2 \frac{(\bar{\rho}_2 + \bar{\rho}_1) \alpha_2 (1 - \alpha_2) \tilde{k}}{\sigma} \quad (18)$$

Note the presence of the two modeling constants in these terms,  $C_1$  and  $C_2$ , respectively. While the first one is directly a constant which smoothly drives the computed  $\Sigma$  toward the equilibrium value, the second one is inversely proportional to the critical Weber number ( $We_c$ ) defined in Duret et al. (2013). The chosen values for these constants ( $C_1 = 1.0$  and  $C_2 = 0.035$ ) come from the configuration presented in Desantes et al. (2017b).

Finally, the  $S_{\Sigma_{init}}$  term is a proper initialization source term, which is necessary due to the fact that all the terms involved in the equation are proportional to the interface surface density ( $\Sigma$ ) and is modeled as in Rachakonda et al. (2016). More details about the previous terms can be found in Pandal et al. (2020a, 2017a, 2017b).

## 2.2. Terminal velocity closure

The solution for the terminal velocity is obtained from the balance with the drag force (Manninen et al., 1996) as follows:

$$|\mathbf{v}_{21,0}| \cdot \mathbf{v}_{21,0} = \frac{V_D}{A_D} \frac{2}{C_d} \frac{\bar{\rho}_2 - \rho_m}{\bar{\rho}_1} \left[ \mathbf{g}_m - (\mathbf{v}_m \cdot \nabla) \mathbf{v}_m - \frac{\partial \mathbf{v}_m}{\partial t} \right] \quad (19)$$

The terminal velocity is proportional to the density difference between the dispersed phase and the surrounding fluid, and to body forces due to local accelerations. In addition,  $\mathbf{v}_{21,0}$  is a function of the drag coefficient ( $C_d$ ), the volume ( $V_D$ ) and the frontal area ( $A_D$ ) of the dispersed phase. Considering the dispersed phase in form of droplets, once the atomization has occurred, the geometrical ratio can be evaluated through the droplet Sauter mean diameter.

$$\frac{V_D}{A_D} = \frac{2}{3} \frac{d_{32}}{\bar{\rho}_2} \quad (20)$$

Finally, taking advantage of the interphase surface area density ( $\Sigma$ ), together with the mass averaged liquid fraction, the local droplet size can be derived, i.e., the local SMD ( $d_{32}$ ):

$$d_{32} = \frac{6}{\bar{\rho}_2} \frac{\rho_m \tilde{Y}_2}{\Sigma} \quad (21)$$

which creates the coupling between the  $\Sigma$  and the  $\tilde{Y}_2$  transport equation.

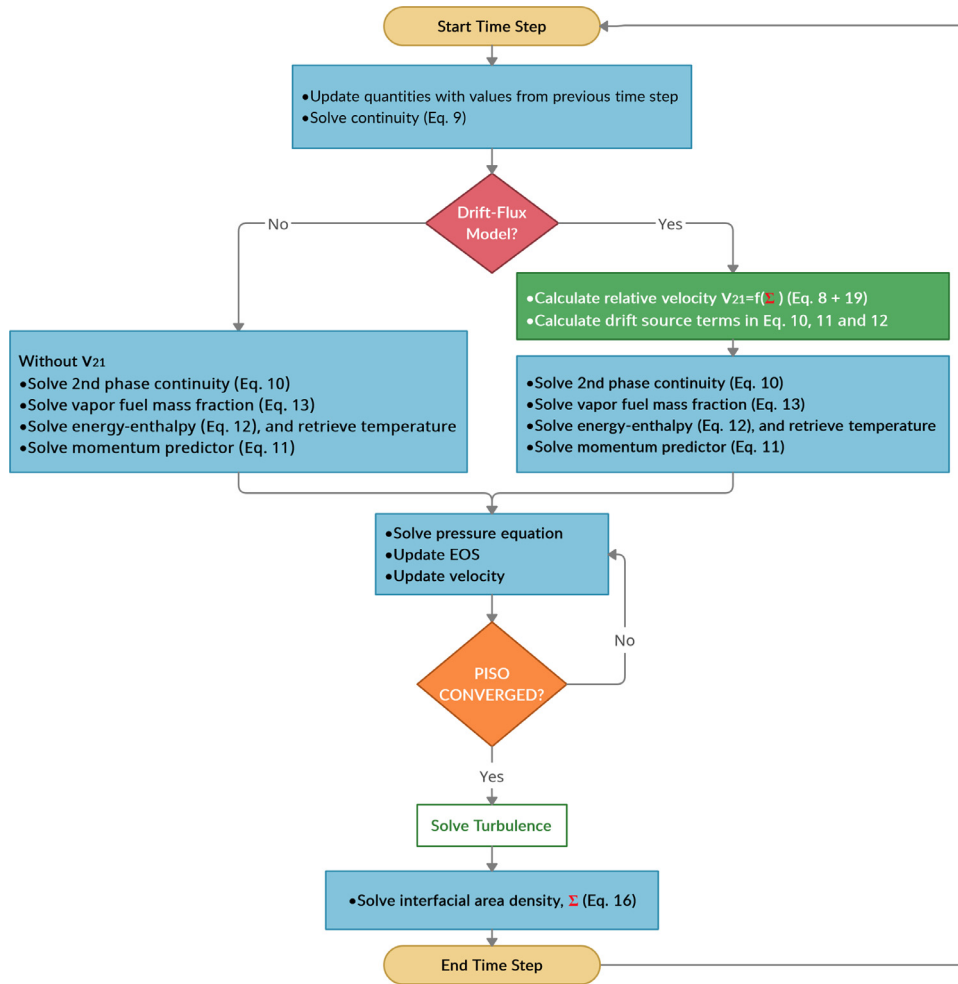


Fig. 1. Flow chart of the new  $\Sigma$ -Y Spray Atomization Model coupled with a Drift-Flux velocity closure.

Table 1  
Model constants for Eq. (22).

Constant	Desantes et al. (2009)	Rusche and Issa (2000)
$K_1$	-0.6	2.1
$K_2$	-1	1
$K_3$	0.25	0.249

Lastly, in order to close the terminal velocity equation, an expression to compute the drag coefficient should be provided. A first basic attempt was evaluated in Pandal et al. (2020b), relying only on the Schiller-Naumann correlation (Schiller and Naumann, 1935). However, for this kind of application it is mandatory to consider the impact of the phase fraction on the drag, because liquid droplets are not isolated. Then, the correlation proposed by Rusche and Issa (2000) is used in the present work (see Eq. (22)). This correlation belongs to the so-called 'new correlations' family, in which a function of the local void fraction ( $\alpha_2$ ) is used as a multiplier of the drag acting on a single dispersed element.

$$C_{d,\alpha_2} = C_d \cdot f(\alpha_2) = C_d \cdot [\exp(K_1\alpha_2) + K_2\alpha_2^{K_3}] \quad (22)$$

However, as indicated by Desantes et al. (2009) the  $C_d$  dependence on the void fraction was derived for dispersed drift-flux, while for diesel sprays different conditions should be taken into account. As a result, constant values for diesel sprays proposed by Desantes et al. (2009) are used (see Table 1):

Regarding the drag coefficient of the isolated particle, the traditional correlation for a spherical body from Schiller and Naumann (1935) is used:

$$C_d = \begin{cases} 0.424, & \text{if } Re \geq 1000 \\ \frac{24}{Re} (1 + 1/6 Re^{2/3}), & \text{otherwise} \end{cases} \quad (23)$$

Finally, in order to compute the Reynolds number, a viscosity value is required. To accomplish this goal, the mixture viscosity concept from Ishii and Zuber (1979) is considered (where the subscripts '1' and '2' refer again to the continuous and dispersed phases, respectively):

$$Re = \frac{\bar{\rho}_1 |\mathbf{v}_{21}| d_{32}}{\mu_m} \quad (24)$$

$$\mu_m = \frac{\mu_1}{(1 - \alpha_2)^{2.5(\mu_2 + 0.4\mu_1)/(\mu_2 + \mu_1)}} \quad (25)$$

### 2.3. Summary of the coupling between $\Sigma$ and the governing equations

In order to clearly highlight that  $\Sigma$  becomes an active scalar in this new formulation, a flow chart of the solution procedure is shown in Fig. 1. At the beginning of each time step, after storing quantities and updating mixture density, if the drift-flux model is used, it is possible to calculate the relative velocity  $\mathbf{v}_{21}$  (Eq. (8)), as the sum of the terminal velocity  $\mathbf{v}_{21,0}$  (Eq. (19)) and of the  $\alpha_2$  gradient contribution. Both terms are evaluated explicitly in the current implementation, therefore using known values of  $\alpha_2$  and  $\mathbf{v}_m$

from the previous time step. Next, the extra terms due to drift, highlighted in the conservation Eqs. (10), (11) and (12), which depend on  $\mathbf{v}_{21}$  or  $\mathbf{v}_{21,0}$ , are evaluated, again explicitly.

Then, the solution procedure follows the usual steps for a segregated pressure-based solver, using the PISO algorithm. After turbulence quantities are evaluated, the  $\Sigma$  equation (Eq. (16)) is finally solved. The interfacial area density is then used to evaluate the Sauter mean diameter  $d_{32}$  (Eqs. (20) and (21)) and the drag coefficient (Eqs. (22)–(25)). This ultimately creates the coupling of  $\Sigma$  to the rest of the conservation equations at the new time step, enabling fully coupled calculations through the drift flux model.

The traditional approach, following the left side of the chart, was not able to carry any information from the interfacial area density back into the main flow variables, thus leaving  $\Sigma$  a passive scalar. The current model on the right side of the chart, instead, is able to actively couple all the transport equations, with a novel formulation that makes  $\Sigma$  an active scalar and solves a long-lasting issue of the  $\Sigma$ -Y model.

#### 2.4. Combustion model

Regarding the combustion model, the strategy followed in this work can be classified as an Unsteady Flamelet / Progress Variable (UFPV) approach. The single-fluid eulerian spray model is coupled with a turbulent combustion model based on the laminar flamelet concept (proposed by Peters, 2000). The complete flamelet model, applied to diesel engine simulations, results in a high computational cost which makes it impractical for such engineering calculations. In this framework, the Approximated Diffusion Flamelet (ADF) approach, where new assumed hypotheses lead to a simplified model which still maintains the physical structure of the flamelet (Michel et al., 2008) has been reported to show satisfactory results (Desantes et al., 2017a; Michel et al., 2008; Payri et al., 2019; Tillou et al., 2014), while maintaining a low computational cost. As a result, it has been chosen in this work to generate the laminar flamelet manifolds. Additionally, the turbulence-chemistry interaction is accounted for by means of a presumed PDF approach (O'Brien, 1980; Pope, 1985). A tabulation technique is adopted to store precalculated turbulent flamelet solutions in order to allow the use of detailed chemical mechanisms at reasonable computational cost.

The present combustion model was originally presented by Winklinger (2014) for Lagrangian spray models, and further developed in recent works (Desantes et al., 2017a; 2020a), while the construction and validation of the coupling methodology with the single-fluid spray model was presented in a previous work (Pandal et al., 2018). Therefore, with the aim of focusing the attention of the present work on the drift-flux model, for a deep description of the numerical implementation of the combustion approach the reader is referred to Pandal et al. (2018).

The target of the present application in reactive conditions is the Engine Combustion Network "Spray A", where n-dodecane is the single fuel species. To this end, the chemical mechanism proposed by Narayanaswamy et al. (2014) is used in this work. Note that this is a skeletal mechanism comprised of 255 species and 2289 reactions to describe n-dodecane chemistry.

### 3. Experimental database

In order to evaluate and validate the  $\Sigma$ -Y Atomization Model coupled with drift-flux closure, two different databases of specific test rigs for diesel spray characterization were considered. Both of them were generated by single-hole axisymmetric nozzles, using a high-pressure common rail system.

For non-vaporizing sprays data from Payri et al. (2008, 2011) have been used. In those experiments, the sprays were in-

**Table 2**

Nozzle geometric characteristics for non-vaporizing tests (CMT nozzle).

D [mm]	L/D [-]	r/D [-]	k-factor
0.112	8.93	0.30	2.8

**Table 3**

Nozzle geometric characteristics for vaporizing sprays (ECN injectors).

Injector Serial #	D [mm]	L/D [-]	r/D [-]	k-factor
210675	0.0894	11.5	0.23	1.3
210677	0.0837	12.3	0.24	1.8

jected into a quiescent vessel where back pressure is modified at constant room temperature, so that ambient densities from 10 to 40  $\text{kg/m}^3$  are obtained in a non-vaporizing environment. Additionally, different injection pressures are available between 30 and 130 MPa.

The nozzle geometry characteristics are summarized in Table 2, where D, L and r denote nozzle orifice outlet diameter, length and inlet radius, respectively. The nozzle convergence is described by the k-factor, as defined in Kastengren et al. (2012), Macián et al. (2003). The orifice is convergent with 0.112 mm outlet diameter and the nozzle was hydro-eroded in order to round the edges of orifice inlet. Both geometric characteristics are aimed to prevent cavitation, as demonstrated by the hydraulic characterization presented in Payri et al. (2012).

Spray macroscopic characteristics, namely penetration and cone angle, have been obtained by high-speed imaging. A detailed description of the experimental set-up and image acquisition methodology can be found in Payri et al. (2011). For the same injector and conditions, an additional source of spray data are the velocity measurements from Payri et al. (2008), performed at different axial sections located from 25 to 50 mm to the orifice. As described in Araneo et al. (2006), a specific optimization of the PDPA system has been performed in order to improve measurements at those conditions.

On the other hand, validation under vaporizing and reacting conditions has been conducted within the frame of the ECN community, specifically with the ECN-Spray A database (ECN, 2018). The 'Spray A' condition consists of a free diesel spray injected into a quiescent environment, where well-defined boundary conditions and experimental data are available for model validation purposes. In the Spray A nominal condition the fuel is n-dodecane, which has a density of 703  $\text{kg/m}^3$  at the experimental conditions. Fuel pressure is set at 150 MPa, ambient temperature at 900 K and the ambient density at 22.8  $\text{kg/m}^3$ . Detailed internal nozzle geometric and hydraulic characterization has been performed (Kastengren et al., 2012), being the main characteristics presented in Table 3 for the two injectors used in the present study. These injectors are characterized by a smooth entrance and strongly convergent angle, which strongly avoid nozzle cavitation, providing a simplification of the nozzle/spray connection.

Additionally to standard spray characterization parameters, a remarkable feature is that local air/fuel ratio measurements have been performed by means of a Rayleigh scattering technique (Pickett et al., 2011). The latter data enable a complete analysis for validation and evaluation of CFD model, both in global and local terms, but these advanced measurements are made for a different Spray A nozzle (210677) and due to this fact, it has been also evaluated with the CFD model.

In addition to nominal condition, a set of parametric variations based on this reference case has been performed (with the injector serial 210675). This includes lower and higher injection pres-

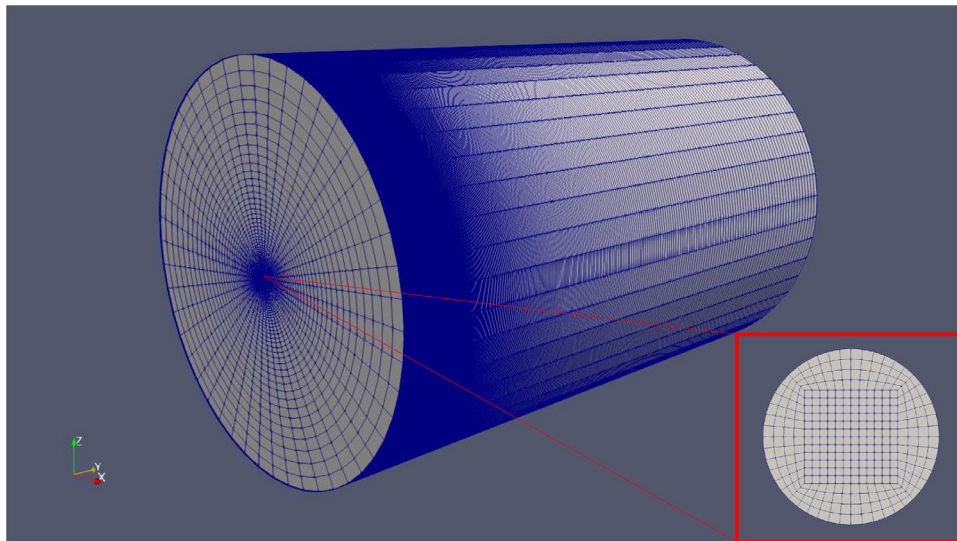


Fig. 2. Computational grid for CFD model simulations. The inset shows the mesh resolution of the nozzle orifice.

Table 4

Simulated Spray A parametric variations studies under vaporizing conditions (Injector serial 210675).

Spray A condition	$P_{inj}$ [MPa]	$T_{amb}$ [K]	$\rho_{amb}$ [kg/m <sup>3</sup> ]
Baseline	150	900	22.8
P1	<b>50</b>	900	22.8
P2	<b>100</b>	900	22.8
D1	150	900	<b>7.6</b>
D2	150	900	<b>15.2</b>
T1	150	<b>700</b>	22.8
T2	150	<b>1000</b>	22.8

Table 5

Simulated Spray A parametric variations studies under reacting conditions (Injector serial 210675).

Condition	D1	D2	Baseline
$P_{inj}$ [MPa]	150	150	150
$T_{amb}$ [K]	900	900	900
$\rho_{amb}$ [kg/m <sup>3</sup> ]	<b>7.6</b>	<b>15.2</b>	<b>22.8</b>
$X_{O_2}$ [%]	15	15	15
ID [ms]	1.93	0.70	0.43
LoL [mm]	59.4	27.9	17.7

sure (P1 and P2) and ambient temperature (T1 and T2), and reductions in ambient density conditions (D1 and D2) as can be seen in Table 4. Model performance is characterized by means of a typical global spray parameter such as liquid and vapor tip penetration and compared against the proper experimental measurements.

Finally, the assessment under reacting conditions is only conducted for the parametric variations of the ambient density. Then, the baseline condition and the two reductions in ambient density (D1 and D2) as can be seen in Table 5. Additionally, in Table 5, typical combustion metrics have been shown for these conditions, namely ignition delay (ID) and lift-off length (LoL) used in order to determine the predictive performance of the model.

#### 4. Numerical model

Only external flow is considered in the present work therefore, in order to simulate the single-hole diesel-like injectors of the present research work, a cylindrical spray chamber with 80 mm in length and 50 mm in diameter is selected as computational domain for CFD calculations. An extended domain reaching 108 mm of ax-

ial extent has been used for including reacting spray development. There are 20 cells across nozzle outlet diameter (O-grid structure), resulting in minimum grid spacing of around 5  $\mu$ m (it varies between both injector nozzle types due to different diameter). The mesh is stretched in axial and radial directions, keeping an aspect ratio close to one in the near nozzle region, with expansion ratios of 1.01 and 1.05 in the axial and radial directions, respectively. This construction results from a grid convergence study and consists of around 400 thousand hexahedral cells, with the structure shown in Fig. 2.

Concerning the boundary conditions, the domain is open at the end of the mesh, while no-slip conditions were selected for the wall of the domain. A non-reflective boundary condition is used for the open outlet and a time varying velocity condition is used for the inlet. The inlet velocity is obtained from mass flow rate and momentum flux measurements (Payri et al., 2005), applying a constant radial profile of axial velocity and density at nozzle outlet. In previous works (Desantes et al., 2016b; Pandal et al., 2018), present configuration has shown remarkable performance.

Regarding turbulence modeling, although a LES approach could be used with  $\Sigma$ -Y model as in Desantes et al. (2020b), present work is focused on the performance of the drift-flux model and thus, a faster and less computationally demanding RANS approach is used to investigate spray development till the combustion process. Then, the k- $\epsilon$  turbulence model was employed for the simulations. Due to the well known round jet spreading overprediction of k- $\epsilon$  type models (Pope, 1978), a corrected value for  $C_{1\epsilon} = 1.60$  is used, as indicated in Desantes et al. (2016a,b). The turbulent intensity was set to 5% (Desantes et al., 2016a; García-Oliver et al., 2013; Lacaze et al., 2015) and the length scale to 10% of the orifice diameter, as suggested in Sallam and Faeth (2003). These values have been proved to be quite reasonable after a sensitivity study conducted in Pandal et al. (2016). Finally, the discretization of the divergence terms is done with a second order Gamma NVD scheme and a first order Euler scheme is applied for time derivative terms.

#### 5. Results and discussion

##### 5.1. Non-vaporizing sprays

In the present section, modeling predictions are compared against CMT measurements of the single-hole nozzle. First, an analysis of spray tip penetration is conducted, to provide an

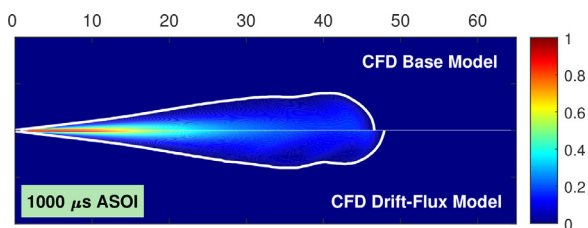


Fig. 3. Computed liquid mass fraction ( $\tilde{Y}_2$ ) contours at 1000  $\mu$ s ASOI.  $P_{inj} = 30$ MPa and  $\rho_{amb} = 10$ kg/m<sup>3</sup>. CFD base model (top) and drift-flux model (bottom).

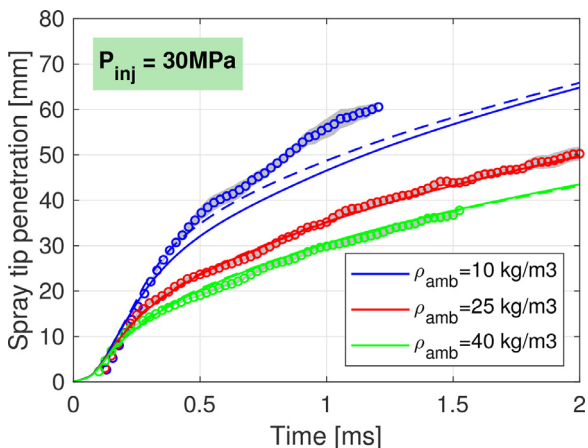


Fig. 4. Computed and measured spray penetration for different ambient density conditions at  $P_{inj} = 30$ MPa. CFD base model predictions (solid line) and drift-flux model predictions (dashed line), experimental measurements (symbols).

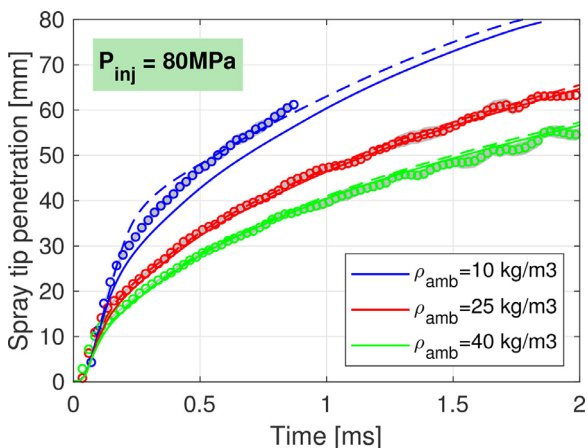


Fig. 5. Computed and measured spray penetration for different ambient density conditions at  $P_{inj} = 80$ MPa. CFD base model predictions (solid line) and drift-flux model predictions (dashed line), experimental measurements (symbols).

overview of the drift-flux model impact. After that, local flow is compared to experiments in terms of centerline velocity. Finally, spray spreading angle modeling predictions are examined for the full range of operating conditions, using both the original and the drift-flux model.

Firstly, an example of model predictions of liquid mass fraction ( $\tilde{Y}_2$ ) is presented in Fig. 3, in the most adverse conditions (low injection pressure and low ambient density). White solid lines correspond to contours of 1% of liquid mass fraction value depicted in order to clearly define spray limits. The longer liquid tip penetration predicted by the new derived model can be noted, together with a narrower spray shape. Further quantitative analyses are conducted in the following.

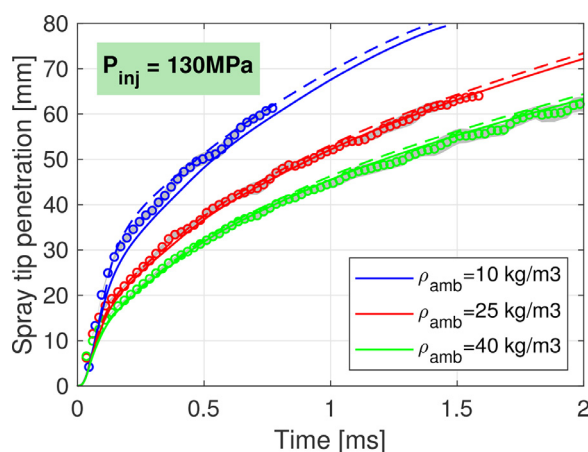
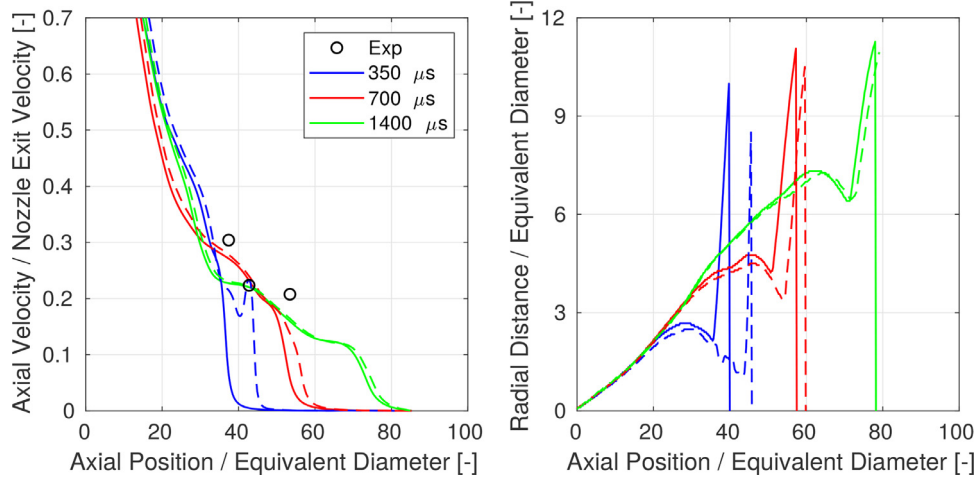


Fig. 6. Computed and measured spray penetration for different ambient density conditions at  $P_{inj} = 130$ MPa. CFD base model predictions (solid line) and drift-flux model predictions (dashed line), experimental measurements (symbols).

In Figs. 4–6, spray penetration predictions are depicted for both the baseline model (solid line) and the new drift-flux one (dashed line) against the experimental measurements. Results are reported grouped by injection pressure conditions and thus, at each level it is visible the lower accuracy of the original model for the lowest ambient density case and additionally, the positive impact of the drift-flux model at those conditions. Overall, although the difference between models is noticeable it may not seem very important. Probably, in these kind of applications the gas surrounding the droplets in the dense zone has been accelerated during the atomization and thus, finally there is not that much of difference between liquid and gas velocities. Other applications like a jet in cross-flow should benefit more from present model. It is also worth restating that the drift effect is linearly correlated with the difference between liquid and gas densities, as expressed by the terminal velocity (Eq. (19)). The results highlight this sensitivity: the new model improves the predictions exactly at those conditions where the original model has more deficiencies.

Independently of the injection pressure condition, at high and mid ambient density the original model performance is fairly accurate, being correctly less affected by drift-flux (slip velocity between phases is less significant at lower liquid-to-gas density ratios). It is at the lowest ambient density conditions that the new model outperforms the original one, almost matching experimental measurements. However, one can observe that the model is not able to improve the spray tip penetration over the whole injection duration, especially at the lowest injection pressure case. The positive impact achieved through the drift velocity progressively vanishes with time and the predicted tip penetration tends towards the one already obtained with the original  $\Sigma$ - $\gamma$  model. As suggested in Pandal et al. (2020b), this is a consequence of an over-predicted coalescence mechanism at the spray tip, and due to that, bigger fuel droplets create a higher drag force which slows down the spray tip penetration. In this regards, a further development of the interphase spray modeling  $\Sigma$  is still needed in order to keep enhancing its predictive capabilities.

Tip spray penetration increase is a consequence of a narrower spray prediction together with higher local velocities. An example of these metrics is depicted in Fig. 7 (for the intermediate injection pressure and lowest ambient density case) in terms of the transient evolution of centerline velocity profiles and the spray radius (according to a spray radial limit defined as the 5% of the on-axis velocity value). Note that normalized velocity and spatial coordinates are used, by scaling in terms of nozzle velocity and equiva-



**Fig. 7.** Time development of computed on-axis velocity [left] and spray radius [right] for  $P_{inj} = 80MPa$  and  $\rho_{amb} = 10kg/m^3$ . CFD base model predictions (solid line), drift-flux model predictions (dashed line).

lent diameter Eq. (26), respectively.

$$d_{eq} = d_0 \sqrt{\rho_{fuel} / \rho_{amb}} \quad (26)$$

In terms of centerline velocity CFD results, along the profile slightly higher velocities are obtained with the drift-flux model although, they are still lower than PDPA measurements. More noticeable is the difference shown at the tip of the spray, which corresponds with a faster penetration. However, it is also possible to observe transition from initial spray development stages ( $350 \mu s$ ), where the drift model shows a greater impact, to the progressive attenuation due to coalescence overestimation. Aside from the increase in local velocity, Fig. 7 (right) depicts a narrower spray in comparison with the original model, in accordance with all the presented results. The same transition seen for on-axis velocity can be observed here. At the first two instants predicted spray is clearly narrower and longer in comparison with original model, while at  $1400 \mu s$  the radial dilation becomes unnoticeable and both models provides almost the same spray.

Continuing the analysis with the intermediate injection pressure and lowest ambient density case, an effort is made to shed some light on how drift-flux affects the spray evolution by means of the analysis of both a CFD contour of the Terminal Velocity ( $v_{21,0}$ ) field and ‘entrainment’, as presented in Fig. 8. In turbulent jets, ‘entrainment’ is the process by which ambient fluid is driven into the jet. As it is already known, this process is a fundamental factor for the growth of direct injection diesel sprays, because it controls the fuel-air mixing rate. It is a parameter traditionally considered for the study of atmospheric gas jets, but recently has caught the attention of both experimentalists (Eagle et al., 2014; García-Oliver et al., 2017) and modellers (Pandal et al., 2018) under diesel engine conditions. Here it will be analyzed by means of CFD predictions. For that purpose, the entrainment coefficient is defined as:

$$C_e(x) = \frac{d\dot{m}_{eq}}{dx \dot{m}_0} \quad (27)$$

where  $\dot{m}$  is the mass flux across a full cross-section of the spray,  $\dot{m}_0$  the mass flux at the orifice,  $x$  the downstream axial distance and  $d_{eq}$  the equivalent diameter. Then, entrainment rate is computed as a function of axial distance, considering that the spray radial limit is located at the radial position where the velocity is equal to 1% of the on-axis velocity.

Regarding the velocity contour Fig. 8 [top], directly related with the additional terms included in the model equations due to drift-flux formulation, one can additionally observe two contours. White

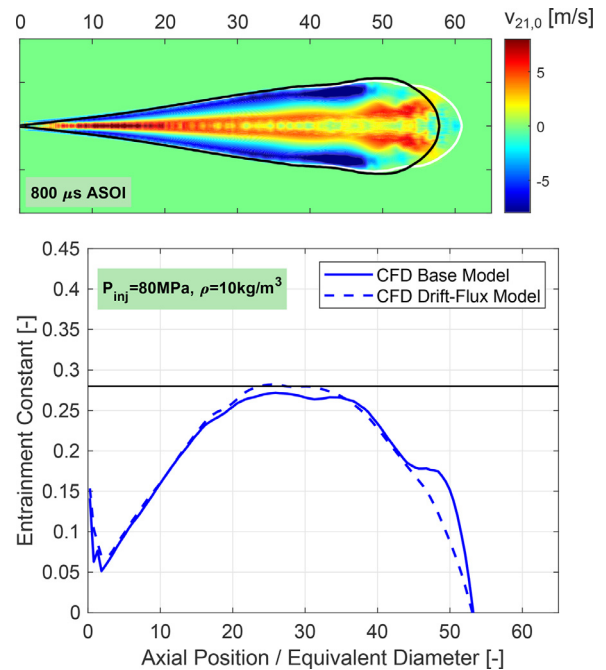


**Fig. 8.** Terminal velocity ( $v_{21,0}$ ) contour at  $800 \mu s$  after SOI [top] and computed entrainment constant [bottom] for base model (solid line) and drift-flux model (dashed line) averaged in the  $350\text{--}1400 \mu s$  interval after SOI. Horizontal line indicates the 0.28 reference value derived from Eagle et al. (2014).  $P_{inj} = 80MPa$  and  $\rho_{amb} = 10kg/m^3$ .

line corresponds to the spray contour predicted by the drift-flux model while the black one is the prediction of the base model, depicted here as a reference. Positive axial terminal velocities at the tip of the spray can be noticed, that drive the penetration towards a larger value when using the drift-flux model. The same conclusion arises from the analysis of entrainment (Fig. 8 [bottom]), where base model results are depicted with a solid line and drift-flux model ones with a dashed line. Here, values have been averaged in the  $350\text{--}1400 \mu s$  interval in order to consider quasi-steady state predictions in a wide extension of the spray. Approaching the tip spray region, lower entrainment value is shown by drift-flux model, which is perfectly in accordance with longer tip penetration. Additionally, after the initial transient region located near the nozzle (below  $20 d_{eq}$ ), a relatively flat evolution can be seen with

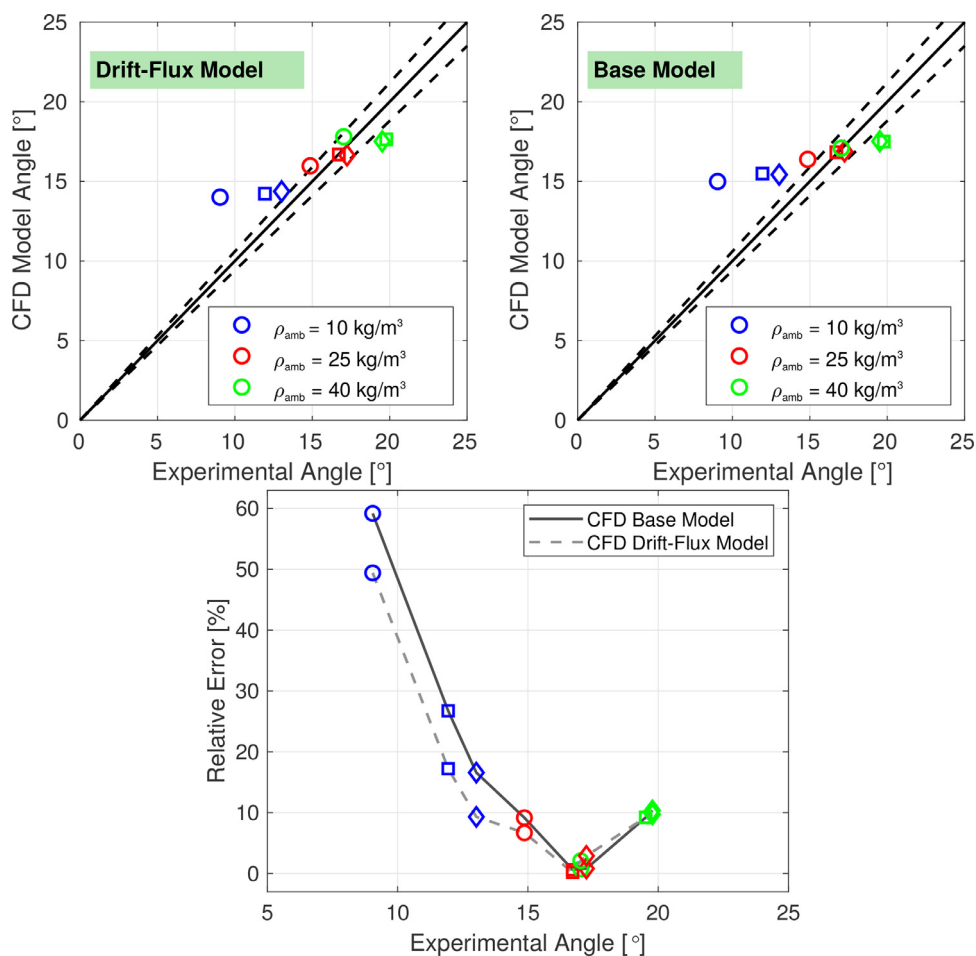


**Fig. 9.** Computed and measured spray angle including a 5% error area (dashed lines) [top] and CFD Relative Error [bottom]: Full matrix of cases studied. Circles ( $P_{inj} = 30MPa$ ), squares ( $P_{inj} = 80MPa$ ) and diamonds ( $P_{inj} = 130MPa$ )

entrainment constant values close to the reference one of 0.28 derived in Eagle et al. (2014), but it is only the drift model that exactly matches it.

The study of macroscopic characteristics includes also the spray angle comparison. This angle is calculated as the time-averaged value included by the lines fitting the two sides of the spray up to 60% of the spray penetration. For that purpose the limit of the spray is defined at the 5% the on-axis mixture fraction value. In Fig. 9 [top], the full matrix of cases simulated is shown for both drift-flux model (left) and Base model (right). Lowest ambient density points with blue symbols, intermediate ambient density points in red and the high ambient density points with green ones. Different symbols are used to represent the different injection pressure conditions, low condition points (circles), intermediate condition (squares) and high condition (diamonds).

In view of the results, the predicted spray angles, in the case of the high and mid ambient density,  $\rho_{amb} = 40kg/m^3$  and  $\rho_{amb} = 25kg/m^3$ , fall within the 5% error of measured values, for some conditions the model underpredicts, for other it overpredicts the experimental values. Additionally, both model performance are almost identical at those conditions. Once again, drift-flux model effect is shown at lowest ambient density conditions. drift-flux model results at ambient density of  $\rho_{amb} = 10kg/m^3$  show fairly good angle predictions, especially improving the two highest injection pressures. Now (with new drift-flux model), for the high and intermediate injection conditions the error is around 10% and 16% respectively, which is a remarkable improvement with respect to the baseline model results of about 16% and 27%. Nevertheless, for

the lowest injection pressure improvement is still not enough to obtain accurate results, showing an error of around a 50% against an original one of 60%, which is in accordance with the penetration shown in Fig. 4. Due to the progressively diminishing impact of the drift, spray tip penetration is slowed down and this is reflected at the spray angle due to its time-averaging process. In any case, model predictions for non-vaporizing conditions show a remarkable improvement in comparison with previous results, encouraging its further development and testing to prove its validity.

### 5.2. Vaporizing sprays

The validation of the model under vaporizing conditions starts with the simulation of the baseline Spray A condition for the injector 210677. This first analysis is made considering to main goals, firstly, to validate the drift-flux model for vaporizing sprays and to establish a first comparison between original and drift-flux model performance. First, similar to the non-vaporizing study, a main contour view of the spray is shown in Fig. 10 where predicted mixture mass fraction by both models could be compared. White solid lines correspond to contours of 1% of the on-axis mixture fraction value, while white dashed line depicts contours of 1% of liquid mass fraction. In this regards, the differences are much more subtle and the quantitative evaluation is required to draw any conclusion. In order to compare modeling predictions with measurements, note here that the computational spray vapor penetration and liquid length are calculated as defined by the ECN (ECN, 2018). The maximum distance from the nozzle outlet to where the fuel vapor

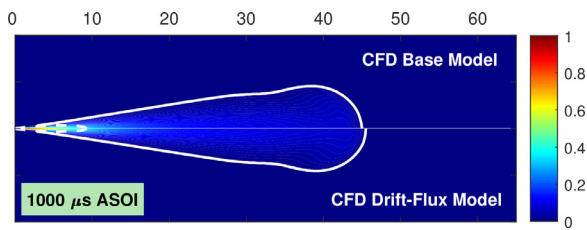


Fig. 10. Computed mixture mass fraction contours at 1000  $\mu$ s ASOI. Spray A Injector 210677,  $P_{inj} = 150$  MPa,  $T_{amb} = 900$  K and  $\rho_{amb} = 22.8\text{kg/m}^3$ . CFD base model (top) and drift-flux model (bottom).

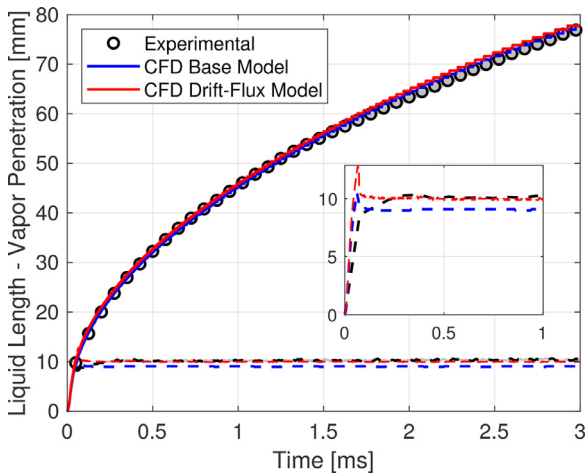


Fig. 11. Computed and measured liquid and vapor penetration. Spray A Injector 210677,  $P_{inj} = 150$  MPa,  $T_{amb} = 900$  K and  $\rho_{amb} = 22.8\text{kg/m}^3$ .

mass fraction is 0.1% and the further distance along the injector axis having a liquid volume fraction higher than 0.1% (Bardi et al., 2012), respectively.

In Fig. 11, spray vapor penetration and liquid length evolution are shown together with an insert focused on the liquid initial evolution. Overall, good agreement is depicted. In terms of vapor penetration, both models seem to provide almost the same prediction falling within the experimental uncertainty of measured values. However, in the case of liquid length, greater differences can be noticed. In this case, while the original model slightly underpredicts the measurements, the drift-flux model matches them show-

ing a clear performance improvement. This is in line with the expected impact of the drift, which is meant to improve the liquid-gas interfacial exchange models.

To conclude model validation, a more detailed investigation is made by quantifying the air/fuel ratio predictions. Rayleigh data are also used to compare predicted vs measured values of mixture fraction, as shown in Fig. 12. Predicted values on the axis, Fig. 12 (left), always fall within the confidence interval of the measurements. It is noticeable a higher prediction by drift-flux model up to about  $45 d_{eq}$ , from this axial position downstream the difference is progressively vanished. This fact is completely coherent with the longer liquid length prediction. In terms of radial dispersion of mixture fraction, results have been plotted in normalized coordinates (i.e. X-axis is the radial divided by the axial coordinates, while the Y-axis is the local mixture fraction divided by the on-axis one). The shape of the profiles is adequately predicted, as shown in Fig. 12 (right). There is a slight bias towards narrower radial profiles in the calculation compared to the experimental ones at both axial locations, which is essentially coherent with the lowest radial dispersion observed in the spray vapor contours.

In essence, modeling performance is not drastically different but drift-flux model provides a better description of the spray by the prediction of a longer liquid length. After this validation process, the assessment of parametric studies with nozzle 210675 is presented in Fig. 13. In these studies only the stabilized value of liquid length is compared against experimental measurements and, once again, base model results are presented to show the actual impact of the drift-flux model. Note that in this analysis, vapor penetration predictions are not shown, as the drift-flux model does not impact the vapor far field according with Fig. 11 [top]. In any case, the model is able to provide accurate predictions for spray vapor penetration trough the whole range of parametric studies as shown in past works (García-Oliver et al., 2013; Pandal et al., 2020a).

Spray liquid length predictions for the parametric studies with different injection conditions have been summarized in Fig. 13 (left). In general, good agreement between calculations and experiments is obtained, although the advantage of the drift-flux model is evidenced. While both models depicts good performance in comparison with experimental measurements, drift-flux model exactly matches experimental trends (slightly decreasing trend with increasing injection pressure) and values. In contrast with a maximum deviation of 5%, for the lowest injection pressure, when the base model is used. It is remarkable that the

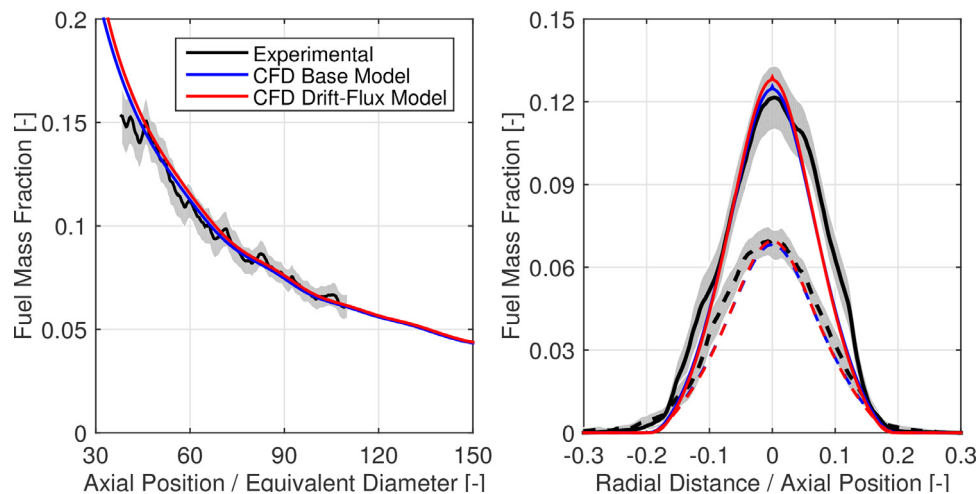


Fig. 12. Computed and measured centerline fuel mass fraction [left] and fuel mass fraction radial profiles  $50 d_{eq}$  (solid line) and  $90 d_{eq}$  (dashed line) [right] at 2.8 ms after SOI. Spray A Injector 210677,  $P_{inj} = 150$  MPa,  $T_{amb} = 900$  K and  $\rho_{amb} = 22.8\text{kg/m}^3$ .

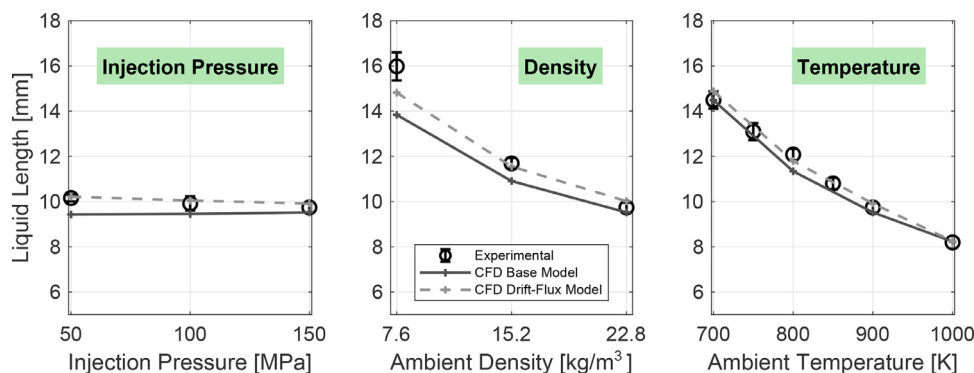


Fig. 13. Computed and measured liquid length values for different parametric variations. Injection pressures (left), ambient densities (center) and ambient temperatures (right). CFD base model predictions (solid line) and drift-flux model predictions (dashed line), experimental measurements (circles). Spray A Injector 210675.

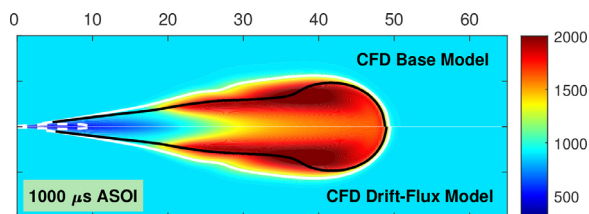


Fig. 14. Computed mean temperature contours at 1000  $\mu$ s ASOI. Spray A Injector 210675,  $p_{inj} = 150$  MPa and  $T_{amb} = 900$  K and  $\rho_{amb} = 22.8$  kg/m<sup>3</sup>. CFD base model (top) and drift-flux model (bottom).

biggest impact occurs for the lowest injection pressure, where injection velocity is lower promoting a greater effect of the slip between phases.

Results for different ambient density conditions are depicted in Fig. 13 (center). The effects of ambient density on quasi-steady values of liquid length are also well predicted. The drift-flux model again outperforms the baseline model results and corrects, to a large extent, the original deviation (baseline model underpredicts the measurement by about a 13% for lowest ambient density) which appears as ambient gas density is decreased (greater density ratio). However, although the prediction is clearly improved, it still shows an underprediction of around 7% for the lowest ambient density, being capable of perfectly matching the measurements at the other two density conditions.

Finally, parametric studies for different ambient temperatures are depicted in Fig. 13 (right). The trends of the quasi-steady liquid length values vs. ambient temperature are very similar to those already observed in previous parametric analyses. Again, an overall great agreement is shown, but drift-flux model always predicts slightly longer liquid lengths, closer to the experimental measurements.

### 5.3. Reacting sprays

In the present section, the drift-flux model performance is finally assessed under reacting conditions and compared against ECN measurements. As it has been verified within this work, the major impact of the drift-flux model occurs for low density conditions and as a result, reacting application is only evaluated for the parametric ambient density variation.

The model assessment begins with the visual comparison of mean temperature contours in Fig. 14 under reacting conditions. White solid lines correspond to contours of 1% of the on-axis mixture fraction value, while white dashed line depicts contours of 1% of liquid mass fraction. In this case, the black line corresponds to the stoichiometric isoline. Both model distributions are quite simi-

lar with the maximum temperature located really close to the stoichiometric isoline towards regions slightly richer. A slightly different tip penetration can be noted as well as a minimal difference on the spray spreading angle.

Moving to the parametric ambient density study, first of all, an analysis of the global combustion parameters is conducted using both CFD models. The two parameters that usually characterize transient reacting diesel sprays are ignition delay (ID) and lift-off length (LoL). Fig. 15 shows both CFD predictions and experimental measurements of these metrics. Regarding modeling results, ECN (ECN, 2018) recommendations are followed, so that ID is defined as the time spent from start of injection (SOI) until the maximum gradient ( $dT/dt$ ) in temperature takes place. On the other hand, LoL is defined as the minimum axial distance to the nozzle where 14% of the maximum value of Favre-average OH mass fraction in the domain is reached (Desantes et al., 2017b; Pei et al., 2016).

Experimental trends followed by both parameters are well-captured by both models providing quite similar results. ID values deviations from experiments are almost inexistent for the two higher ambient density conditions, while moderate for lowest ambient density. This latter operating point is where the impact of drift-flux model becomes noticeable, however it is not sufficient to provide a remarkable modeling performance. This sort of disagreement with experiments has also been observed with the present combustion model and a lagrangian spray description (Desantes et al., 2017a), and is mainly due to the strong role of chemical mechanism on the exact ignition timing. On the other hand, LoL is clearly underpredicted as the ambient density is decreased. The effect of the drift-flux model on reactive conditions, although noticeable and in the correct direction, is very small.

In order to understand the reason why the positive impact created by drift-flux model on the simulated results vanishes under reacting spray conditions, entrainment is again analysed. Computed local entrainment rate results are shown in Fig. 16 for baseline Spray A condition simulated by both CFD models, original model (solid line) and drift-flux model (dashed line). Values have been averaged in the 2800–4050  $\mu$ s interval in order to ensure quasi-steady state predictions in a wide extension of the spray. Axial extension is clipped at 60  $d_{eq}$  because the effect of the transient tip of the spray affects entrainment values downstream of this axial position. Additionally to entrainment inert and reacting profiles, measured values of liquid length and LoL are depicted by means of two black vertical lines, dotted and dashed, respectively. Independently of the chosen profile, one can observe a first transient region located near the nozzle (below 20  $d_{eq}$ ), where  $C_e(x)$  has a lower value in agreement to results in Han and Mungal (2001), Hill (1973) because of the transition between the nozzle and the fully developed turbulent spray. After that, and fo-

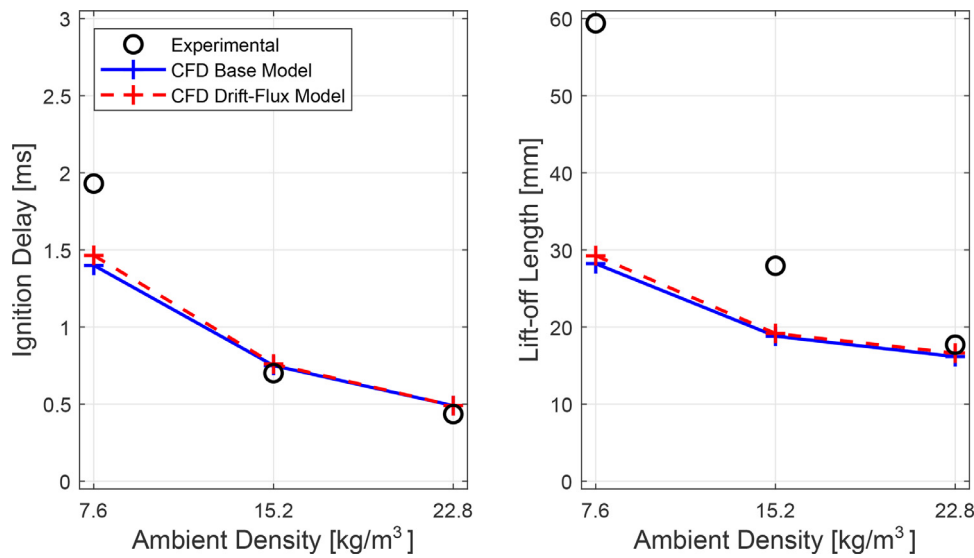


Fig. 15. Computed and measured ignition delay (left) and lift-off length position (right) for different ambient density conditions. CFD base model predictions (solid line) and drift-flux model predictions (dashed line), experimental measurements (circles). Spray A Injector 210675,  $P_{inj} = 150$  MPa and  $T_{amb} = 900$  K.

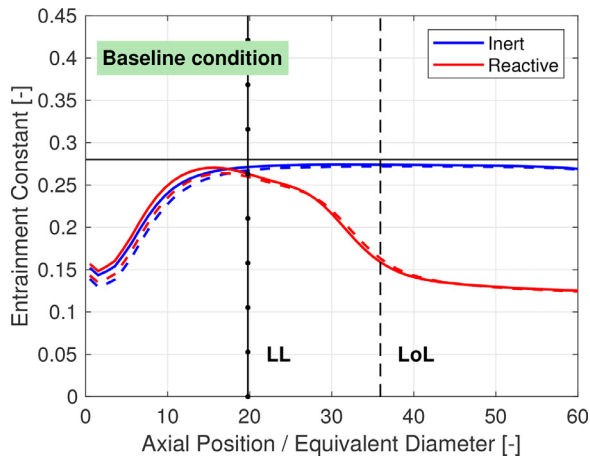


Fig. 16. Computed entrainment constant for base model (solid line) and drift-flux model (dashed line) for inert and reacting conditions averaged in the 2800–4050  $\mu$ s interval after SOI. Vertical dashed line indicates the LoL location while dotted line indicates the liquid length. Horizontal line indicates the 0.28 reference value derived from Eagle et al. (2014). Baseline Spray A condition,  $P_{inj} = 150$  MPa,  $\rho_{amb} = 22.8$  kg/m<sup>3</sup> and  $T_{amb} = 900$  K.

ocusing on the inert spray, a relatively flat evolution can be seen with a value quite near to the reference one of 0.28 derived in Eagle et al. (2014). Moving to reacting conditions, the entrainment rate profile is mainly the same as the inert one within the first transition region. Then, its evolution presents a decay (around a 50%) which starts in between the liquid length and LoL locations. Apart from the extremely similar profiles obtained by both Eulerian models, the interesting point is that the drift-flux model creates an entrainment reduction within the first region of the spray (below 20  $d_{eq}$ ). Comparing inert and reacting conditions, one can see that lower entrainment of the drift-flux model is kept even downstream of the liquid length location while it is lost during the decay of the reacting profile. This fact provides an additional interpretation regarding the impact of the model on the liquid length, which becomes longer due to less air entrainment, while reacting sprays are not affected. The same overall behavior is observed for the other two operating conditions which were evaluated.

### 6. Summary and conclusions

A complete validation of a new developed and coupled  $\Sigma$ -Y Spray Atomization Model that accounts for diffusion due to drift-flux velocities is presented in this work. The new model has been applied to non-vaporizing, vaporizing and reacting diesel-like fuel sprays under different test conditions, which cover a wide range of injection pressures and ambient gas densities.

In non-vaporizing conditions, the validation of the new model has been conducted through comparison against measurements of different spray metrics such as tip penetration, centerline velocity and spray cone angle. Model predictions are also compared to the results of the original model, without drift-flux correction. Tip penetration rates predictions are in very good agreement with the experimental data under medium and high ambient gas density conditions, where both models provide almost identical results. However, for the lowest ambient gas density drift-flux formulation provides a remarkable improvement for the three injection pressures evaluated, as a result of a higher degree of slip between velocities. Only for lowest injection pressure, the positive impact progressively vanishes with time as a consequence of an overpredicted coalescence mechanism at the spray tip. The effect is noticeable in the transient evolution of the centerline velocity profiles. Additionally, spray cone angle predictions are greatly enhanced, especially at low density conditions, with a relative error reduction of 10% for the low-density low-injection pressure condition.

Validations under vaporizing conditions for the ECN spray A injector has shown quite similar spray behavior except for the greater liquid length and slightly higher spray velocity values, as expected from previous studies. However, major impact has been observed on the exploration of different conditions around the spray A baseline case. Results prove that the drift-flux has a good impact on the liquid behavior and beyond the liquid length vapor is not much affected, therefore the model becomes insensitive. This is justifiable, because vapor diffusion itself is not changed, especially for spray A, where liquid penetrates only marginally into the far field. Regarding reacting conditions, model captures experimental trends of ID and LoL, although quantitatively not much improved in comparison with original model. This was somewhat expected for ID, because it is mainly determined by the chemical mechanism. Probably, tested condition for which there is great physical space between liquid and combustion regions have made

impossible to catch a deeper impact on the combustion and maybe a larger nozzle could be more interesting for future investigations. These conclusions have been confirmed with the entrainment rate analysis for each vaporizing-reacting pair of conditions. While lower entrainment, that allows longer penetration, is maintained slightly downstream of the liquid length position for vaporizing conditions when drift-flux is used, under reacting conditions the effect vanishes earlier of the LoL location. This fact, at the moment, precludes the possibility of effectively studying the impact of the new developed drift-flux  $\Sigma$ -Y model on combustion, and assessing if additional benefits could be obtained. Further work will be needed in this regard and maybe other two-phase flow test cases, like jets in cross-flow could be studied in the future, to further assess the validity of the drift-flux model.

In summary, the new drift-flux  $\Sigma$ -Y model construction has proven its full validity with a remarkable performance improvement for inert environments in both cold and hot conditions, while it has seemed almost insensitive under reacting conditions for which weaker interaction between liquid fuel and combustion takes place. With that being said, the main contribution of this work is on proposing a model for fully coupling liquid dispersion and spray atomization and thus, any development of the  $\Sigma$  model formulation can potentially enhance predictive capabilities, overcoming a traditional limitation of the single-fluid  $\Sigma$ -Y model.

### Declaration of Competing Interest

The authors declare that they have no known competing financial interests or personal relationships that could have appeared to influence the work reported in this paper.

### CRediT authorship contribution statement

**A. Pandal:** Conceptualization, Methodology, Software, Validation, Formal analysis, Investigation, Resources, Data curation, Writing - original draft, Writing - review & editing, Visualization, Project administration, Funding acquisition. **B.M. Ningegowda:** Writing - review & editing. **F.N.Z. Rahantamialisoa:** Writing - review & editing, Investigation. **J. Zemi:** Writing - review & editing. **H.G. Im:** Supervision, Project administration, Funding acquisition. **M. Battistoni:** Conceptualization, Methodology, Validation, Formal analysis, Investigation, Resources, Writing - review & editing, Supervision, Project administration, Funding acquisition.

### Acknowledgement

Authors acknowledge that part of this work was partially funded by Banco Santander in the frame of 'ayudas económicas de movilidad de excelencia para docentes e investigadores de la Universidad de Oviedo, 2019' and by Universidad de Oviedo in the frame of 'Modalidad B: Ayudas para proyectos de Equipos de Investigación emergentes 2020' under the project *Modelos de Interfaz Difusa en Sprays para Plantas Propulsivas Sostenibles (DIFFIST)*.

The support from King Abdullah University of Science and Technology, Saudi Arabia, under the CRG grant OSR-2017-CRG6-3409.03, is also gratefully acknowledged.

### References

Andreini, A., Bianchini, C., Puggelli, S., Demoulin, F., 2016. Development of a turbulent liquid flux model for Eulerian-Eulerian multiphase flow simulations. *Int. J. Multiph. Flow* 81, 88–103. doi:10.1016/j.ijmultiphaseflow.2016.02.003.

Araneo, L., Soare, V., Payri, R., Shakal, J., 2006. Setting up a PDPA system for measurements in a diesel spray. *J. Phys.* 45, 85–93.

Bardi, M., Payri, R., Malbec, L., Bruneaux, G., Pickett, L., Manin, J., Bazyn, T., Genzale, C., 2012. Engine combustion network: comparison of spray development, vaporization, and combustion in different combustion vessels. *Atomization Sprays* 22 (10), 807–842.

Battistoni, M., Magnotti, G.M., Genzale, C.L., Arienti, M., Matusik, K.E., Duke, D.J., Giraldo, J., Ilavsky, J., Kastengren, A.L., Powell, C.F., Marti-Aldaravi, P., 2018. Experimental and computational investigation of subcritical near-nozzle spray structure and primary atomization in the engine combustion network spray D. *SAE Int. J. Fuels Lubr.* 11, 337–352. doi:10.4271/2018-01-0277.

Battistoni, M., Som, S., Powell, C.F., 2019. Highly resolved Eulerian simulations of fuel spray transients in single and multi-hole injectors: nozzle flow and near-exit dynamics. *Fuel* 251, 709–729. doi:10.1016/j.fuel.2019.04.076.

Beau, P.-A., Funk, M., Lebas, R., Demoulin, F.-X., 2005. Applying quasi-multiphase model to simulate atomization processes in diesel engines: modeling of the slip velocity. SAE Technical Paper. SAE International doi:10.4271/2005-01-0220.

Beau, P.A., Lebas, R., Funk, M., Demoulin, F.X., 2004. A multiphase flow approach and a single-phase flow approach in the context of a euler model for primary break-up. In: *ILASS2004 - 19th European Conference on Liquid Atomization and Spray Systems*, September 6–8, Nottingham, UK.

Blokkeel, G., Barbeau, B., Borghi, R., 2003. A 3D Eulerian model to improve the primary breakup of atomizing jet. SAE Technical Paper. SAE International doi:10.4271/2003-01-0005.

Crua, C., Manin, J., Pickett, L.M., 2017. On the transcritical mixing of fuels at diesel engine conditions. *Fuel* 208, 535–548. doi:10.1016/j.fuel.2017.06.091.

Dahms, R.N., Manin, J., Pickett, L.M., Oefelein, J.C., 2013. Understanding high-pressure gas-liquid interface phenomena in diesel engines. *Proc. Combust. Inst.* 34 (1), 1667–1675. doi:10.1016/j.proci.2012.06.169.

Dahms, R.N., Oefelein, J.C., 2015. Liquid jet breakup regimes at supercritical pressures. *Combust. Flame* 162 (10), 3648–3657. doi:10.1016/j.combustflame.2015.07.004.

Desantes, J., García-Oliver, J., Novella, R., Pérez-Sánchez, E., 2017a. Application of an unsteady flamelet model in a RANS framework for spray a simulation. *Appl. Therm. Eng.* 117, 50–64. doi:10.1016/j.applthermaleng.2017.01.101.

Desantes, J., García-Oliver, J., Novella, R., Pérez-Sánchez, E., 2020. Application of a flamelet-based CFD combustion model to the LES simulation of a diesel-like reacting spray. *Comput. Fluids* 200, 104419. doi:10.1016/j.compfluid.2019.104419.

Desantes, J., García-Oliver, J., Pastor, J., Olmeda, I., Pandal, A., Naud, B., 2020. LES Eulerian diffuse-interface modeling of fuel dense sprays near- and far-field. *Int. J. Multiph. Flow* 103272. doi:10.1016/j.ijmultiphaseflow.2020.103272.

Desantes, J., Payri, R., Salvador, F., Gil, A., 2006. Development and validation of a theoretical model for diesel spray penetration. *Fuel* 85 (7), 910–917. doi:10.1016/j.fuel.2005.10.023.

Desantes, J.M., García-Oliver, J.M., Pastor, J.M., Pandal, A., 2016. A comparison of diesel sprays CFD modelling approaches: DDM vs  $\Sigma$ -Y Eulerian atomization model. *Atomization Sprays* 26 (7), 713–737. doi:10.1615/AtomizSpr.2015013285.

Desantes, J.M., García-Oliver, J.M., Pastor, J.M., Pandal, A., Baldwin, E., Schmidt, D.P., 2016. Coupled/decoupled spray simulation comparison of the ECN spray a condition with the  $\Sigma$ -Y Eulerian atomization model. *Int. J. Multiph. Flow* 80, 89–99. doi:10.1016/j.ijmultiphaseflow.2015.12.002.

Desantes, J.M., García-Oliver, J.M., Pastor, J.M., Pandal, A., Naud, B., Matusik, K., Duke, D., Kastengren, A., Powell, C., Schmidt, D.P., 2017. Modelling and validation of near-field diesel spray CFD simulations based on the  $\Sigma$ -Y model. In: *ILASS2017 - 28th European Conference on Liquid Atomization and Spray Systems*, September 6–8, Valencia, Spain doi:10.4995/ILASS2017.2017.4715.

Desantes, J.M., Margot, X., Pastor, J.M., Chavez, M., Pinzello, A., 2009. CFD-phenomenological diesel spray analysis under evaporative conditions. *Energy Fuels* 23 (8), 3919–3929. doi:10.1021/ef9002999.

Dukowicz, J.K., 1980. A particle-fluid numerical model for liquid sprays. *J. Comput. Phys.* 35 (2), 229–253. doi:10.1016/0021-9991(80)90087-X.

Duret, B., Reveillon, J., Menard, T., Demoulin, F., 2013. Improving primary atomization modeling through DNS of two-phase flows. *Int. J. Multiph. Flow* 55, 130–137. doi:10.1016/j.ijmultiphaseflow.2013.05.004.

Eagle, W.E., Musculus, M.P.B., Malbec, L.M., Bruneaux, G., 2014. Measuring transient entrainment rates of a confined vaporizing diesel jet. In: *ILASS Americas 26th Annual Conference on Liquid Atomization and Spray Systems*.

ECN, 2018. Engine combustion network data archive URL <http://www.sandia.gov/ecn/>.

Faeth, G.M., 1983. Evaporation and combustion of sprays. *Prog. Energy Combust. Sci.* 9 (1–2), 1–76. doi:10.1016/0360-1285(83)90005-9.

García-Oliver, J.M., Pastor, J.M., Pandal, A., Trask, N., Baldwin, E., Schmidt, D.P., 2013. Diesel spray CFD simulations based on the  $\Sigma$ -Y Eulerian atomization model. *Atomization Sprays* 23, 71–95.

García-Oliver, J.M., Malbec, L.-M., Toda, H.B., Bruneaux, G., 2017. A study on the interaction between local flow and flame structure for mixing-controlled diesel sprays. *Combust. Flame* 179, 157–171. doi:10.1016/j.combustflame.2017.01.023.

Gorokhovski, M., Herrmann, M., 2008. Modeling primary atomization. *Annu. Rev. Fluid Mech.* 40 (1), 343–366. doi:10.1146/annurev.fluid.40.111406.102200.

Guan, L., Tang, C., Yang, K., Mo, J., Huang, Z., 2015. Effect of di-n-butyl ether blending with soybean-biodiesel on spray and atomization characteristics in a common-rail fuel injection system. *Fuel* 140, 116–125. doi:10.1016/j.fuel.2014.09.104.

Han, D., Mungal, M., 2001. Direct measurement of entrainment in reacting/nonreacting turbulent jets. *Combust. Flame* 124 (3), 370–386. doi:10.1016/S0010-2180(00)00211-X.

Hill, B.J., 1973. Measurement of local entrainment rate in the initial region of axisymmetric turbulent air jets. *J. Fluid Mech.* 51 (4), 773–779. doi:10.1017/S0022112072001351.

Ishii, M., Hibiki, T., 2006. *Thermo Fluid Dynamics of Two Phase Flow*. Springer, New York doi:10.1007/978-0-387-29187-1.

- Ishii, M., Zuber, N., 1979. Drag coefficient and relative velocity in bubbly, droplet or particulate flows. *AIChE J.* 25 (5), 843–855. doi:10.1002/aic.690250513.
- Jedelsky, J., Maly, M., del Corral, N.P., Wigley, G., Janackova, L., Jicha, M., 2018. Air-liquid interactions in a pressure-swirl spray. *Int. J. Heat Mass Transf.* 121, 788–804. doi:10.1016/j.ijheatmasstransfer.2018.01.003.
- Kastengren, A., Ilavsky, J., Viera, J.P., Payri, R., Duke, D., Swantek, A., Tilocco, F.Z., Soavis, N., Powell, C., 2017. Measurements of droplet size in shear-driven atomization using ultra-small angle x-ray scattering. *Int. J. Multiph. Flow* 92, 131–139. doi:10.1016/j.ijmultiphaseflow.2017.03.005.
- Kastengren, A., Tilocco, F.Z., Powell, C.F., Manin, J., Pickett, L.M., Payri, R., Bazyn, T., 2012. Engine combustion network (ECN): measurements of nozzle geometry and hydraulic behavior. *Atomization Sprays* 22, 1011–1052.
- Lacaze, G., Misdariis, A., Ruiz, A., Oefelein, J.C., 2015. Analysis of high-pressure diesel injection processes using LES with real-fluid thermodynamics and transport. *Proc. Combust. Inst.* 35 (2), 1603–1611. doi:10.1016/j.proci.2014.06.072.
- Lebas, R., Menard, T., Beau, P.A., Berlemont, A., Demoulin, F.X., 2009. Numerical simulation of primary break-up and atomization: DNS and modeling study. *Int. J. Multiph. Flow* 35, 247–260.
- Lee, C.H., Reitz, R.D., 2013. Cfd simulations of diesel spray tip penetration with multiple injections and with engine compression ratios up to 100:1. *Fuel* 111, 289–297. doi:10.1016/j.fuel.2013.04.058.
- Ma, P.C., Wu, H., Banuti, D.T., Ihme, M., 2019. On the numerical behavior of diffuse-interface methods for transcritical real-fluids simulations. *Int. J. Multiph. Flow* 113, 231–249. doi:10.1016/j.ijmultiphaseflow.2019.01.015.
- Macián, V., Bermúdez, V., Payri, R., Gimeno, J., 2003. New technique for determination of internal geometry of a diesel nozzles with the use of silicone methodology. *Exp. Tech.* 37, 39–43.
- Manninen, M., Taivassalo, V., Kallio, S., 1996. *On the Mixture Model for Multiphase Flow*. VTT Julkaisija Utgivare Publisher.
- Michel, J.-B., Colin, O., Veynante, D., 2008. Modeling ignition and chemical structure of partially premixed turbulent flames using tabulated chemistry. *Combust. Flame* 152 (1), 80–99. doi:10.1016/j.combustflame.2007.09.001.
- Mo, J., Tang, C., Li, J., Guan, L., Huang, Z., 2016. Experimental investigation on the effect of n-butanol blending on spray characteristics of soybean biodiesel in a common-rail fuel injection system. *Fuel* 182, 391–401. doi:10.1016/j.fuel.2016.05.109.
- Narayanawamy, K., Pepiot, P., Pitsch, H., 2014. A chemical mechanism for low to high temperature oxidation of n-dodecane as a component of transportation fuel surrogates. *Combust. Flame* 161 (4), 866–884. doi:10.1016/j.combustflame.2013.10.012.
- O'Brien, E.E., 1980. *The Probability Density Function (pdf) Approach to Reacting Turbulent Flows*. Springer Berlin Heidelberg, Berlin, Heidelberg, pp. 185–218. doi:10.1007/3540101926\_11.
- Pandal, A., García-Oliver, J.M., Novella, R., Pastor, J.M., 2018. A computational analysis of local flow for reacting diesel sprays by means of an Eulerian CFD model. *Int. J. Multiph. Flow* 99, 257–272. doi:10.1016/j.ijmultiphaseflow.2017.10.010.
- Pandal, A., García-Oliver, J.M., Pastor, J.M., 2020. Eulerian CFD modeling of nozzle geometry effects on ECN sprays A and D: assessment and analysis. *Int. J. Engine Res.* 21 (1), 73–88. doi:10.1177/1468087419882500.
- Pandal, A., Pastor, J.M., García-Oliver, J.M., Baldwin, E., Schmidt, D.P., 2016. A consistent, scalable model for Eulerian spray modeling. *Int. J. Multiph. Flow* 83, 162–171. doi:10.1016/j.ijmultiphaseflow.2016.04.003.
- Pandal, A., Pastor, J.M., Payri, R., Kastengren, A., Duke, D., Matusik, K., Giraldo, J.S., Powell, C., Schmidt, D., 2017. Computational and experimental investigation of interfacial area in near-field diesel spray simulation. *SAE Int. J. Fuels Lubr.* 10 (2). doi:10.4271/2017-01-0859.
- Pandal, A., Payri, R., García-Oliver, J.M., Pastor, J.M., 2017b. Optimization of spray break-up CFD simulations by combining  $\Sigma$ -Y Eulerian atomization model with a response surface methodology under diesel engine-like conditions (ECN Spray A). *Comput. Fluids* 156, 9–20. doi:10.1016/j.compfluid.2017.06.022.
- Pandal, A., Rahantamalisoa, F., Ningegowda, B. M., Battistoni, M., 2020b. An Enhanced  $\Sigma$ -Y Spray Atomization Model Accounting for Diffusion Due to Drift-Flux Velocities. *SAE Technical Paper 2020-01-0832*. 10.4271/2020-01-0832
- Payri, F., García-Oliver, J.M., Novella, R., Pérez-Sánchez, E.J., 2019. Influence of the n-dodecane chemical mechanism on the CFD modelling of the diesel-like ECN spray a flame structure at different ambient conditions. *Combust. Flame* 208, 198–218. doi:10.1016/j.combustflame.2019.06.032.
- Payri, R., García, J., Salvador, F., Gimeno, J., 2005. Using spray momentum flux measurements to understand the influence of diesel nozzle geometry on spray characteristics. *Fuel* 84 (5), 551–561. doi:10.1016/j.fuel.2004.10.009.
- Payri, R., Salvador, F., Gimeno, J., Garcia, A., 2012. Flow regime effects over non-cavitating diesel injection nozzles. *Proc. IMechE Part D* 226, 133–144.
- Payri, R., Salvador, F., Gimeno, J., Novella, R., 2011. Flow regime effects on non-cavitating injection nozzles over spray behavior. *Int. J. Heat Fluid Flow* 32 (1), 273–284. doi:10.1016/j.ijheatfluidflow.2010.10.001.
- Payri, R., Tormos, B., Salvador, F., Araneo, L., 2008. Spray droplet velocity characterization for convergent nozzles with three different diameters. *Fuel* 87 (15), 3176–3182. doi:10.1016/j.fuel.2008.05.028.
- Pei, Y., Hawkes, E.R., Bolla, M., Kook, S., Goldin, G.M., Yang, Y., Pope, S.B., Som, S., 2016. An analysis of the structure of an n-dodecane spray flame using TPDF modelling. *Combust. Flame* 168, 420–435. doi:10.1016/j.combustflame.2015.11.034.
- Peters, N., 2000. *Turbulent Combustion*. Cambridge Monographs on Mechanics. Cambridge University Press doi:10.1017/CBO9780511612701.
- Pickett, L., Manin, J., Genzale, C., Siebers, D., Musculus, M., Idicheria, C., 2011. Relationship between diesel fuel spray vapor penetration/dispersion and local fuel mixture fraction. *SAE Int. J. Engines* 4, 764–799. doi:10.4271/2011-01-0686.
- Pickett, L., Manin, J., Kastengren, A., Powell, C., 2014. Comparison of near-field structure and growth of a diesel spray using light-based optical microscopy and x-ray radiography. *SAE Int. J. Engines* 7 (2).
- Pitzer, K.S., Lippmann, D.Z., Jr., R.F.C., Huggins, C.M., Petersen, D.E., 1955. The volumetric and thermodynamic properties of fluids. II. Compressibility factor, vapor pressure and entropy of vaporization. *J. Am. Chem. Soc.* 77 (13), 3433–3440. doi:10.1021/ja01618a002.
- Pope, S., 1978. An explanation of the turbulent round-jet/plane-jet anomaly. *In: AIAA*, 16, pp. 279–281.
- Pope, S., 1985. Pdf methods for turbulent reactive flows. *Prog. Energy Combust. Sci.* 11 (2), 119–192. doi:10.1016/0360-1285(85)90002-4.
- Rachakonda, S., Wang, Y., Schmidt, D.P., 2016. Flash Boiling: A Parametric Study. *In: ILASS Americas 28th Annual Conference on Liquid Atomization and Spray Systems*.
- Reid, R.D., Prausnitz, J.M., Poling, B.E., 1987. *The Properties of Gases and Liquids*. McGraw-Hill.
- Rusche, H., Issa, R., 2000. The effects of voidage on the drag force on particles, droplets and bubbles in dispersed two-phase flow. *In: Proc. 2nd Japanese-European Two-Phase Flow Group Meeting*. Tsukuba (Japan)
- Sallam, K.A., Faeth, G.M., 2003. Surface properties during primary breakup of turbulent liquid jets in still air. *AIAA J.* 41 (8), 1514–1524.
- Schiller, L., Naumann, Z., 1935. A drag coefficient correlation. *Zeitschrift des Vereines Deutscher Ingenieure* 77, 318–320.
- Schmidt, D.P., Corradini, M.L., 2001. The internal flow of diesel fuel injector nozzles: a review. *Int. J. Engine Res.* 2 (1), 1–22. doi:10.1243/1468087011545316.
- Shin, D.-h., Sandberg, R.D., Richardson, E.S., 2017. Self-similarity of fluid residence time statistics in a turbulent round jet. *J. Fluid Mech.* 823, 1–25. doi:10.1017/jfm.2017.304.
- Siebers, D., 1998. Liquid-phase fuel penetration in diesel sprays. *Trans. SAE* 107, 1205–1227.
- Siebers, D.L., 1999. Scaling liquid-phase fuel penetration in diesel sprays based on mixing-limited vaporization. *Trans. SAE* 108, 703–728.
- Siebers, D.L., 2008. Recent developments on diesel fuel jets under quiescent conditions. *In: Arcoumanis, C., Kamimoto, T. (Eds.), Flow and combustion in reciprocating engines*. Springer-Verlag, Berlin, pp. 257–308.
- Simonin, O., 1990. Eulerian formulation for particle dispersion in turbulent two-phase flows. *In: Proc. 5th Workshop on Two-Phase Flow Predictions*. Erlangen, pp. 156–166.
- Tillou, J., Michel, J.-B., Angelberger, C., Veynante, D., 2014. Assessing LES models based on tabulated chemistry for the simulation of diesel spray combustion. *Combust. Flame* 161 (2), 525–540. doi:10.1016/j.combustflame.2013.09.006.
- Vallet, A., Borghi, R., 1999. Modélisation Eulerienne de l'atomisation d'un jet liquide. *C.R. Acad. Sci., Paris* 327, 1015–1020.
- Vallet, A., Burluka, A.A., Borghi, R., 2001. Development of a Eulerian model for the "atomization" of a liquid jet. *Atomization Sprays* 11 (6).
- Weller, H., Tabor, G., Jasak, H., Fureby, C., 1998. A tensorial approach to computational continuum mechanics using object-oriented techniques. *Comput. Phys.* 12, 620–631.
- Winklinger, J., 2014. *Implementation of a combustion model based on the flamelet concept and its application to turbulent reactive sprays*. Departamento de Máquinas y Motores Térmicos, Universidad Politécnica de Valencia, España Ph.D. thesis.